Operational strategies to improve the performance and long-term cyclability of intermediate temperature sodium-sulfur (IT-NaS) battery

Sathiyaraj Kandhasamy,*[a] Georgios Nikiforidis,[b,c] Gert Jan Jongerden,[d] Ferdy Jongerden,[d] Mauritius C. M. van de Sanden,[a,e] and Mihalis N. Tsampas*[a]

[a] Dr. S. Kandhasamy, Prof. M. C. M. van de Sanden, Dr. M. N. Tsampas
Dutch Institute for Fundamental Energy Research (DIFFER)
Eindhoven, 5612 AJ, The Netherlands
E-mail: S.Kandhasamy@differ.nl; M.Tsampas@differ.nl
[b] Dr. G. Nikiforidis
Laboratory of Physico-Chemistry of Materials and Electrolytes for Energy
University of Tours
Tours, 37071, France
[c] Dr. G. Nikiforidis
LE STUDIUM Institute for Advanced Studies,
Orléans, 45000, France
[c] Dr. G. J. Jongerden, F. Jongerden
Exergy Storage Components and Systems,
Arnhem, 6827 AV, The Netherlands
[e] Prof. M. C. M. van de Sanden
Department of Applied Physics,
Eindhoven University of Technology,
Eindhoven, 5612 AP, The Netherlands

Keywords: Sodium-sulfur (NaS) battery • Solid-state electrolyte interface • Glyme based liquid cathode • Intermediate-temperature (IT) battery • Sulfur utilization

Abstract: Based on the preliminary investigation of the intermediate temperature sodium-sulfur (IT-NaS) battery (150 °C), herein we advance this energy storage system, by re-tuning the catholyte formulation; namely i) concentration, ii) layer thickness and iii) cut-off limits during galvanostatic charge-discharge cycling, lowering the operating temperature and improving cell design. The systematic implementation of these strategies boosted the cell performance markedly, delivering 112 mAh/g-sulfur, 90% of its theoretical specific capacity (125 mAh/g-sulfur), and 50 deep reversible charge-discharge cycles with coulombic and round-trip energy efficiencies of 97 ± 3% and 73 ± 4%, respectively. Along with the stability and improvement of cycle life, this study demonstrates, for the first time, the practicality of the tubular IT-NaS technology at a temperature as low as 125 °C.

1. Introduction

The reduction in the cost of secondary battery systems, primarily Li-ion battery (LIB), renders the integration of battery electrochemical energy storage systems practical at an industrial and residential scale. Yet, the main elements of the LIB, namely lithium, cobalt, and nickel are scarce. Therefore, a potential upsurge in the criticality of these materials can prime the demand in supply, create uncertainty, and could increase the overall cost of LIB in the near future. In search of an alternative, the battery technologies based on sulfur (S) and sodium (Na) show great potential.[1–3] For instance, sodium-sulfur (NaS) batteries with molten Na and S electrodes separated by a β″ alumina solid electrolyte (BASE) are commercially available since three decades ago.[3,4] Japan's NaS battery manufacturer NGK, installed the world's largest battery storage unit (i.e., 648 MWh) in the United Arab Emirates using this technology in 2019. Its storage capacity is five times larger than Tesla's Hornsdale battery (based on LIB technology) installed in Australia a year before.[5] The NaS battery operation principally necessitates a high temperature (HT) (~350 °C) for melting the polysulfides in the cathode, raising safety and financial concerns, and in turn, hindering its wider applicability.[6]

On a non-commercial basis, numerous battery chemistries at lower operating temperatures have flourished. They are intrinsically safe, cheaper, compatible with a wide range of materials for casing and sealants, and more flexible in terms of applicability. A prime exemplar is the NaS room temperature (RT-NaS) cell[2,7,8], which imitates the lithium-sulfur (LiS) battery technology. Here, metallic Na serves as the anode and sulfur as the cathode, the Na ions (Na^+) intercalate/de-intercalate between the two sides of the battery upon charge/discharge. Other than the identical construction and operational chemistry, the RT-NaS is stippled with loss of cathodic active material due to polysulfide shuttling and cell shorting by anodic dendrite growth, hindering its performance and cycle life.[3,4] The RT-NaS technology adopted the Na^+ conducting solid electrolyte (BASE) as a separator, first implemented in commercialized HT-NaS cells.[8,9] Along with high ionic (Na^+) and low electronic conductivity, the BASE possesses a high relative density, mechanical stability, and durability against corrosive melts, producing a remarkable cell lifetime for the HT-NaS (viz. 15 years and up to 4,500 cycles at full power).[6,10] It is immersed in the organic electrolyte between the anode and cathode, alleviating shuttling and dendrite growth. Still, the Na^+ conductivity decreases significantly (BASE's Na^+ conductivity at 25 °C is 1.7 mS/cm[11]) and adds extra resistance to the RT cell.[12] With the above in mind, intermediate temperature (IT) NaS batteries operable at 150 °C aspire to combine the best of both HT and RT NaS technologies.[13–17]

The IT-NaS adopted an analogous tubular configuration to the HT-NaS with the BASE solid separator in-between central anode and outer cathode.[18] The commercialized HT-NaS and Zebra battery technologies prefer the central sodium anode to be encapsulated by tubular BASE than the stacked planner cell designed with flat plate BASE, owing to safety reasons and simplified manufacturing process.[19] To reduce the operating temperature, the cathodic side of IT-NaS was altered by pre-solvating the sulfur/polysulfide mixture in an organic solvent analogous to the one used in RT-NaS's electrolytes.[13,14,16] The selection of suitable organic solvent and co-solvent with adequate solubility for sulfur/polysulfide is of paramount importance, together with thermal, chemical, and electrochemical stability.[17,20] More precisely, having the BASE within the interface of anode-electrolyte-cathode mitigates polysulfide shuttling and dendrite growth; meanwhile, the operating temperature of IT-NaS improves the BASE's Na^+ conductivity (BASE's Na^+ conductivity at 100 and 200 °C are 16.7 and 100 mS/cm, respectively[11]).

We recently reported an IT-NaS battery operating at 150 °C, with a tetraethylene glycol dimethyl ether (TEGDME) solvated sulfur/polysulfide catholyte. A lab-scale IT-NaS cell (Figure S1a) containing 2.5M Na_2S_5 delivered a nominal discharge capacity of 185 mAh[14] and a specific discharge capacity of ~90 mAh/g-sulfur, lower than the theoretical limit, suggesting an ineffective utilization of S. The same was also evident in a larger cell (scale-up cell provided by our industrial partner "Exergy") developed for the same catholyte. Both our lab and scaled-up IT-NaS cells adopt a configuration analogous to the HT-NaS, which is a tubular BASE separator. The sceptic lies on that the liquid state catholyte in IT-NaS is going to facilitate the integration of the flowable catholyte in the future to achieve higher volumetric capacity and energy density, mimicking the technology of redox flow batteries.[16] The volumetric capacity (mAh/ml-catholyte) of the scaled-up cell did not scale up uniformly with the larger catholyte volume.[14]

But interestingly, the scale-up cell exhibited a comparatively lower internal resistance at the initial stages of cycling compared to the lab-scale cell. Since the cell casing material, BASE tube, and catholyte composition (2.5M Na_2S_5 in TEGDME) were the same, we attribute this discrepancy to the different configurations of the cells. The scale-up cell comprises stainless steel (SS) mesh (50% porous) wound around the BASE tube, held next to the BASE surface by a spiral of tungsten wire, and used as a cathodic current collector while on the contrary, in the lab-scale cell, the cell's outer metal casing (3 mm away from the BASE) served as the cathodic current collector. Surely, the change in the cathodic current collector's positioning might attend to the scale-up cell having a low internal resistance by establishing a higher current density distribution at the BASE-catholyte interface.

Ergo, the principal aim of this study is to delineate the impact of cell configuration on battery performance and internal resistance. To this end, the IT-NaS lab cell is carefully reconfigured. At the same time, the catholyte's composition and in-cell properties are re-tuned to enhance cathodic S utilization and long-term stability at 125 °C, which is beneficial to the safety and cost of this battery energy storage system. These optimizations boosted the battery's performance to deliver 90% of its achievable theoretical specific capacity (125 mAh/g-sulfur) for 50 deep charge-discharge cycles.

2. Results and Discussion

2.1. Reconfigured lab-scale IT-NaS cell

Initially, we reconfigured the lab-scale cell (Figure 1a) and wound the SS mesh around the central BASE tube to use it as the cathodic current collector. The reconfigured cell's voltage profile containing 2.5M Na_2S_5 is given in Figure 1b. It operated with identical conditions to the ones reported in our previous study.[14] The cell temperature is 150 °C, and the charge-discharge current density ± 2.5 mA/cm^2. Nearing the charging cut-off limit (2.6 V), the voltage profile for cycle-A shows a significant increase in the cell potential. Discharge starts at 1.9 V and stabilizes at a potential close to the open-circuit voltage (OCV, 2.06 V) before dropping down to the cut-off potential (1.8 V). The shift in cell potential at the end of charge and beginning of discharge is indicative of high cell resistance in these regions, leading to low reversibility (i.e., ~46% coulombic efficiency).[21] The sodium-sulfur electrochemical decoupling chemistry hints the formation (i.e., phase segregation) of S during deeper charging states, augmenting the cell resistance.[13]

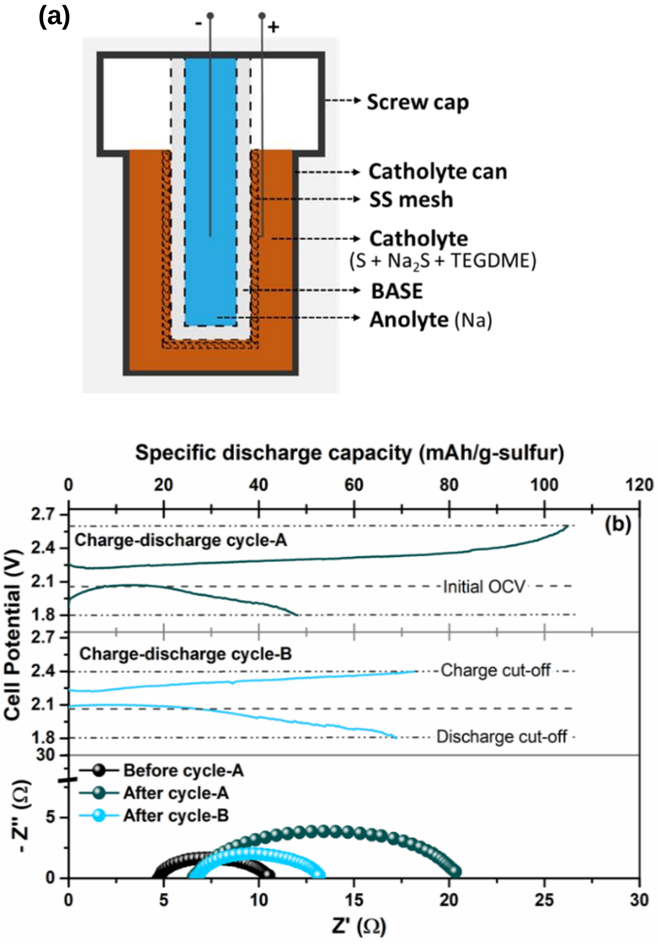

Figure 1. a) Reconfigured lab-scale cell with SS mesh around the BASE, contains initial catholyte of 2.5M Na_2S_5 and **b)** its Nyquist plots at 150 °C.

To overcome this issue, for cycle-B (Fig 1b), the charging cut-off was intentionally limited to 2.4 V. Henceforth, no severe shift in cell potential is evidenced, with the cell being electrochemically reversible and reaching 97 ± 3% coulombic efficiency. HT-NaS cells undergo a supplementary charge method to avoid excessive energy loss due to a drastic rise in internal resistance.[22,23] This method controls the applied charge current density and reduces it to a lower value after reaching a specific potential during charging so as to decelerate the formation rate of insulating S to avoid a rapid increase in cell resistance. Thus, the above finding (Figure 1a & b) confirms that the formation of insulating S during charging prompts the cell for a sudden rise in resistance and hinders its performance.

The EIS spectra (Fig 1b) represented as a single broad semicircle further corroborate our hypothesis. They were recorded for the cell at its initial state (before cycle-A charging), after cycle-A discharge, and after cycle-B discharge. The x-axis intercept (Z') at high-frequency depicts the ohmic resistance (R_{HF}). It includes the resistance contribution from the catholyte, BASE electrolyte, anodic, and cathodic current collectors, and connecting leads.[24] Among these, the most significant contribution (about 95%) stems from the catholyte, as detailed in the SI (equation S1 & Figure S2).[24,25] The difference in Z' between its x-axis intercepts at the high and low frequencies refers to the charge-transfer resistance (R_{LF}) at the current collector interface.[24] Low internal resistance is observed at the reconfigured cell's initial state after the initial conditioning (i.e., before cycle-A). Yet, after the cycle-A discharge, a rise in both R_{HF} and R_{LF} is evident (Table 1). The R_{HF} values after cycle-A and cycle-B discharge are similar. A reduction in R_{LF} is observed after cycle-B discharge, ascribed to the regulated charging cut-off limit that prevents the formation (phase segregation) of insulating S at the current collector interface. Still, R_{HF} and R_{LF} after cycle-B discharge remain larger (43% and 14%, respectively) than at its initial state. The voltage profile of cycle-B shows a shift in the potential of the discharge plateau to a higher potential than the initial OCV, signifying the occurrence of permanent, irreversible loss of active species even before cycle-B. The peak representing the insulating S (i.e., S_8) gets intense for recovered (after cycle-B) catholyte's Raman spectrum (Figure S3) than the initial, again specifies the formation of S at deeper charging state of cycle-A.

We initially selected concentrated catholytes to boost the S concentration (for example, 2.5M Na_2S_5 contain 12.5M S),[14] anticipating a high specific capacity due to the high theoretical capacity of S. Yet, higher concentrations hinder the effective utilization of S in the catholyte,[14,16] possibly exceeding the solubility limit that could saturate the excess S to become inactive. Yang et. al.,[16] reported a substantial decrease in discharge capacity from 850 to 490 mAh/g-sulfur for an increased S concentration from 10 to 20M. In that sense, fine-tuning the initial catholyte recipe is indispensable to find the right balance between the quantity and utilization efficacy of S.

Table 1. Analysis summary of the Nyquist plots in Figure 1b (fitted to the equivalent circuit in Figure S4).

Cell state during the EIS measurements	Resistance (Ω)	
	R_{HF}	R_{LF}
Initial (before cycle-A)	4.7 ± 0.12	5.7 ± 0.21
After cycle-A	6.4 ± 0.13	13.9 ± 0.23
After cycle-B	6.6 ± 0.20	6.5 ± 0.31

2.2. Insight into the catholyte's chemistry for refining its concentration

Ethers are one of the best serving electrolyte solvents in LiS and RT-NaS batteries.[12,26–28] TEGDME, due to its long ether chain, possesses high thermal stability (boiling point 285 °C). This long-chain of ethers is coordinated with five periodic binding sites (i.e., oxygen) with donor nature.[29] Each TEGDME molecule enforces a strong solvent-solute interaction through these sites by framing an open-ended crown to cage a single Na^+ from solvated sodium polysulfides (Na_2S_x), as shown in Figure S5.[27,30,31] Additionally, the solvent's donor number (DN) is critical in attaining chemical disproportionation intermediates during cycling.[28] In the HT-NaS cell, the reduction mechanism is purely electrochemical. During discharge, the S (or S_8) at the cathode reduces to a high order polysulfide (Na_2S_8) and follows a sequence to lower the order to reach Na_2S_4, reversed on charging. Whereas in LiS and RT-NaS cells, the presence of solvent in the electrolyte mediates several chemical disproportionation reactions together with the electrochemical redox reactions.[32–34]

The low DN of TEGDME (18.6)[32] favors the formation of S_4^{2-} (i.e. Na_2S_4) as a disproportionation reaction following the electrochemical reduction of S_8 to S_8^{2-} (i.e. Na_2S_8).[28] On the contrary, a high DN (viz. 28 for dimethyl sulfoxide - DMSO) formulates S_6^{2-} (Na_2S_6) chemically by a disproportion reaction during the reduction of S_8 to S_8^{2-} (Na_2S_8), following the acid-base equilibrium chemistry.[26,28] A hard base like S_4^{2-} is more stable in a weakly solvated Na^+ (hard acid) medium due to low DN. S_6^{2-} is a soft base that stabilizes in a soft acidic medium with strongly solvated Na^+ due to high DN solvent.[26,28] Dissolution of high order polysulfides in such solvents has been conveyed in LiS and RT-NaS batteries as the cause for the shuttling effect.[4,35] On the other hand, within the catholyte, the TEGDME solvent is polar aprotic, while Na_2S and S are polar and apolar, respectively. Polar solvents dissolve polar molecules better than apolar ones. Hence, the solubility of S in TEGDME is limited.[36] Lu et.al.,[15] measured a maximum concentration of ~2.3M of elemental S that could be dissolved in TEGDME at 150 °C. This amount matches a similar finding of another comparable solvent DMAC (N, N-dimethylacetamide), at the same temperature (~2.4M S).[17]

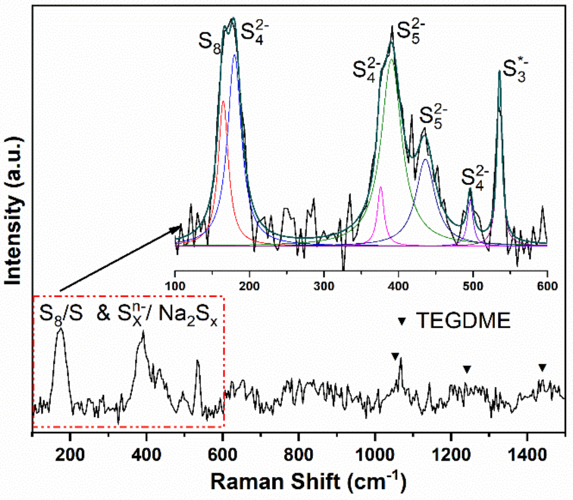

Figure 2. Raman spectrum of the redefined initial catholyte (0.5M Na_2S_5 in TEGDME). Inset shows the fingerprint region for sulfur (S) and sodium polysulfides (Na_2S_x), peaks fitted for additional details.

As alluded to previous reports,[15,17] for better solubility of S in TEGDME, the initial catholyte was diluted to 0.5M Na_2S_5 (containing a total of 2.5M S). Figure 2 shows the Raman spectra of the as-prepared catholyte comprising 0.5M Na_2S_5 in TEGDME. The peaks at the low Raman shift region (150 - 550 cm^{-1}) describe the fingerprint region for the S and Na_2S_x (x = 1 - 8).[37–39] TEGDME contributes to the peaks observed beyond this region (viz. 1000-1500 cm^{-1}).[37] The stoichiometry of the composition promotes the Na_2S_5 phase, depicted by the broad peak between 350 and 450 cm^{-1}, in line with other reports.[15,37–40] The sharp peak observed at 534 cm^{-1} denotes the existence of trisulfide monoanionic radical (S_3^{*-}).[41] In the solutions of polysulfide dianions (S_x^{2-} i.e. Na_2S_x with x = 2 - 5) in donor solvents, the trisulfide monoanionic radical (S_3^{*-}) is formed as a dissociate species on disproportionation reaction to form (1/4)S_8 and S_6^{2-}.[33] These disproportionated species and trisulfide radical chemically recombine back to formulate S_8 for further electrochemical reduction.[33,41,42] On top of Na_2S_5, the above-mentioned acid-base equilibrium in the presence of TEGDME leads to the formation of the stable Na_2S_4 phase with S (a form of S_8), balancing the Na_2S_5 stoichiometry.[15] Peaks related to lower-order polysulfides beyond Na_2S_4 were not observed. The acquired Raman spectra confirm the complete chemical dissolution reaction towards the formation of Na_2S_5.

2.3. Impact of reduction in operating temperature on catholyte's stability and conductivity

The IT-NaS cells operated at 150 °C opted for TEGDME to be the solvent of choice because of its high thermal stability (boiling point is 285 °C).[14–16] Kartal et. al.,[43] determined the thermal stability of the TEGDME in a mixture with different salts by thermogravimetric analysis (TGA). They observed mixture mass loss at 160 °C attributed to the evaporation of TEGDME, even though the temperature is below its boiling point.[43] This leads to the assumption that its low flashpoint (141 °C) propagates this early evaporation. Hence, it is essential to lower the cell operating temperature below TEGDME's flashpoint to protect the catholyte's thermal stability. Yet, we should bear in mind that the temperature cannot fall lower than the melting temperature of S (115 °C). The latter is apolar and not readily dissolved in a polar solvent like TEGDME. Sustaining the cell above 115 °C mitigates the solidification of any unreacted/undissolved S in the catholyte. Accordingly, the practical threshold temperature window for operationally of the cell lies between 115 and 141 °C. The additional reduction in cell temperature will improve safety and diminish the cost of thermal management.

Next, we measured the conductivity (Figure S6a) of the catholytes (ranging from 0.5 to 2.5M Na_2S_5) at two temperatures (125 and 135 °C) within the above predicted practical threshold temperature window (115 to 141 °C) by using a conductance cell. The conductivities were determined by using the solution resistance (R_S, the high-frequency x-axis intercept, Figure S6b) and a pre-determined cell constant (equation S2 in SI).[44] From Figure S6a, the conductivity increases with higher Na_2S_5 concentrations and elevated temperature. For instance, for a concentration of 2.5M, the 10 °C rise amplified the conductivity from 4.7 ± 0.06 to 6.4 ± 0.04 mS/cm, ascribed to a reduction in activation energy for ionic dissociation that provoked higher mobility for the current-carriers.[30]

However, the electrolytic conductivity is not a suitable metric to compare solutions that vary in concentration. The term conductivity (mS/cm) describes the conductance, mobility of ions in the solution in-between electrodes separated by 1 cm apart and having an area of 1 cm^2. But here, the solution chemistry differs by its concentration, which varies in the concentration of ions and the number of charge carriers.[45,46] Thus, it was restated to a comparable specific conductivity quantity, called molar conductivity (Figure 3).[47,48] The value of molar conductivity is equivalent to the conductance caused by all the mobile ionic charge-carriers in the solution reduced to 1M concentration, but for the same volume (cm^3) in-between the electrodes (area 1 cm^2 and 1 cm apart).

Typically, an increase in the solute concentration in a solvent tends to reduce the molar conductivity. At higher concentrations, the degree of ionic dissociation reduces, and the available number of current-carrying ions per unit volume decreases.[30] But Figure 3 shows the molar conductivity increases with an increase in Na_2S_5 concentration initially (at 125 °C rises from 2.14 to 2.76, for 0.5 to 1 M) and drops after reaching a maximum at 1M. Such a behavior has been observed for solutions comprising solvents with low dielectric constant like TEGDME (ε_r = 7.9).[32] The formation of larger aggregates increases the molar conductivity to a maximum during an initial increase in concentration. Augmenting the concentration to 2.5M strengthens the ionic interaction of the aggregates and reduces the mobility of the ionic current-carriers.[49] Macroscopically visualized, a rise in the viscosity of the catholyte enacts it to behave like an ionic liquid.[48] The above finding benchmarks the catholyte concentration to 1M, and within this limit, the conductance doesn't vary significantly for the measured temperatures (125 and 135 °C). Therefore, the optimum temperature for cell operation was chosen as 125 °C.

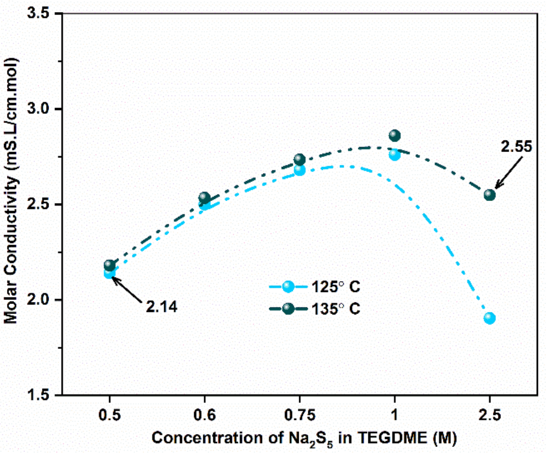

Figure 3. Molar conductivity of the as-prepared catholytes with different Na_2S_5 concentrations in TEGDME.

2.4. Approach to implement the revised charge-discharge cut-off limit

The criteria expected to boost the cell's long-term performance and catholyte stability are (i) reducing the catholyte concentration (<1M Na_2S_5), (ii) lowering the cell temperature to 125 °C, and (iii) narrowing the cut-off limit during charging (i.e. electrochemical oxidation). While the first two can be readily implemented, the determination of the cut-off charging limit proves more challenging but is theoretically possible.[10,50,51] Here, we postulate that the solvation effect and intermediate chemical dissolution of the catholyte could significantly deviate from the practical limits.[20,33] To this end, we implement electrochemical impedance spectroscopy (EIS), a non-invasive technique capable of monitoring the state of charge/discharge and state of health of the battery.[52,53] In the NaS system, the chemical composition of the catholyte follows a sequential reversible change on electrochemical charge/discharge.[8,53] The EIS data revealed that the catholyte contributes heavily to the ohmic resistance (Figure S2 & equation S1).[24,25] So, knowing the tendency in conductivity of the catholyte at its different chemical composition during electrochemical charging and interpreting it through the EIS spectra at different states of charge, we can identify an adequate cut-off endpoint.

The conductivity of the initial catholyte (0.5M Na_2S_5) and its chemical intermediates (i.e., 0.31M Na_2S_8, 0.65M Na_2S_4) on the electrochemical charge-discharge track are visualized in Figure 4, at 125 °C. Across these chemical compositions (Table 2), the content of S (2.5M) remains the same, the only variant being the content of Na^+. During charging, the catholyte's conductivity increases upon the formation of Na_2S_8. Extending the charging process beyond Na_2S_8 will hamper the conductivity on account of the formation of the insulating S (S_8) phase.[53] Upon subsequent discharge, the conductivity decreases, signifying the electrochemical reduction of Na_2S_8 to Na_2S_5 and then to Na_2S_4.[54]

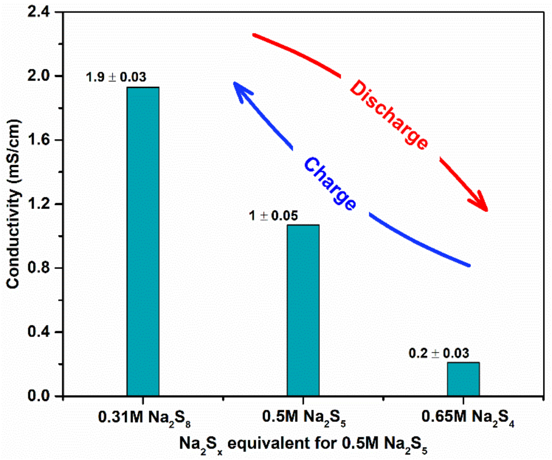

Figure 4. Conductivity at 125 °C of the initial catholyte (0.5M Na_2S_5) and its chemical phases (polysulfide order) on the track of the electrochemical charge-discharge.

Table 2. Catholyte formulation stoichiometry from initial to other equivalents, chemical intermediate compositions on the electrochemical charge-discharge track.

Catholyte Na_2S_x in TEGDME	Formulation composition		Content	
	Na_2S (M)	S (M)	Na (M)	S (M)
0.31M Na_2S_8	0.31	2.19	0.63	2.5
0.5M Na_2S_5	0.5	2	1	2.5
0.65M Na_2S_4	0.65	1.88	1.25	2.5

A cell containing 0.5M Na_2S_5 in TEGDME is subjected to EIS measurements throughout periodic intermediate stages (labeled C_1 to C_5) of galvanostatic charging, as illustrated in Figures 5a & b. The detailed procedure of the combined charge-discharge and EIS measurements is discussed in SI. The ohmic part (x-axis intercept at high frequency) decreases during charging (Figure 5b) until C_3, in line with the conductivity data.[24,25] Going beyond C_3, the cell impedance increases, possibly due to the conversion of Na_2S_8 into S_8. On setting back to discharge from C_5 (D_0) to D_4 (Figure S7), the intermediate EIS and OCV show a reverse tendency to the charging process. The discharge step to D_5 is quickly terminated due to the cut-off potential (1.2 V) but compared to the EIS at D_4, the impedance of D_5 decreases marginally. We postulate that a portion of the chemical species in the catholyte is electrochemically reduced to low order polysulfides beyond Na_2S_4 upon reaching D_4. These species return to TEGDME's chemically favorable stable phase (Na_2S_4) during the intermediate rest periods and produce low impedance at D_5.

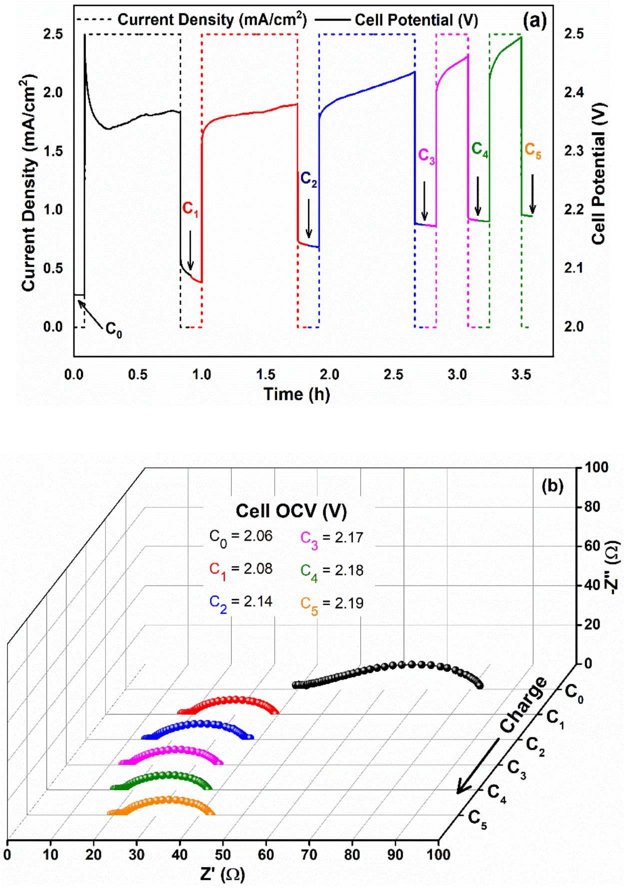

Figure 5. EIS at various intermediate stages on electrochemical charge for a cell with diluted catholyte operated at 125 °C. **a)** Galvanostatic charge voltage and current profile, **b)** EIS spectra.

The data gleaned from Figure 5 endorse this cell for long-term galvanostatic cycling at ± 2.5 mA/cm^2 with the cut-off time limit of 135 minutes, that is, the time to reach C_3. The OCV lies between 2.06 and 2.17 V on charging (Figure 5) and 2.06 V upon subsequent discharge (Figure S7). The charge-discharge cycle is limited within Na_2S_5 and Na_2S_8, leading to a theoretical capacity of 125 mAh/g-sulfur.[3,55,56] Following the initial conditioning process, the EIS spectra of Figure 5 can delineate the practical cut-off limit, which will be combined with the practical limits of the cells to give a long cycle of life.

2.5. Reconfigured lab-scale cell operated under the re-tuned conditions

A cell identical to the one of Figure 1a is assembled, containing 0.5M Na_2S_5, operating at 125 °C and following the cut-off time limit as determined in the previous section ($Na_2S_5 \leftrightarrow Na_2S_8$). For the initial cycle (Figure 6a), the cell delivered a higher specific capacity (~10 mAh/g-sulfur) than the identical cell with concentrated (2.5M) catholyte (Figure 1b, cycle-B). Still, it remains lower than the target-specific capacity (125 mAh/g-sulfur). Up to 20 cycles, the cell is fully reversible. At the 21st cycle, the charge and discharge processes reach the cut-off potential well before the prescribed time, inducing a sudden drop in specific capacity (almost to half). An increase in total cell resistance by ~18% is evident after 21 cycles (Figure 6a). The cause for this rise in resistance is discussed later in section 2.5.

The EIS spectra after the 1st discharge show a second semicircle in the higher frequency region. To extract the relevant information, we used an equivalent circuit with an additional resistive component, R_{MF} (Figure S4).[57,58] Therefore, R_{HF}, R_{MF}, and R_{LF} correspond to the x-intercepts at high, mid, and low frequencies, respectively. They refer to the ohmic resistance (R_{HF}), BASE-catholyte interfacial resistance (R_{MF}), and charge-transfer resistance at the current collector interfaces (R_{LF}). We formulated the equivalent circuit accordingly and ascribed the rise in resistance to the formation of a resistive layer at the BASE-catholyte interface.

The redox reaction of the catholyte is expected to take place at the vicinity of the BASE-catholyte (Na_2S_x)-cathodic current collector (like a three-phase interface).[59] During charging, the Na^+ moves to the anode via the BASE from the catholyte by electrochemically oxidizing low-order Na_2S_x to higher-order ones. To realize this process, the Na_2S_x species consume electrons from the cathodic current collector and move to the BASE surface, where they decouple the Na^+ from the S-S chain, as detailed in HT-NaS.[13] The reconfigured cell (shown in Figure 1a) used for the measurements in Figure 6a has the SS mesh wound around the BASE tube, with a separation of less than 0.2 mm. Positioning the cathodic current collector closer to the BASE surface enables a higher current density distribution in that vicinity (i.e., three-phase interface) than in the bulk of the catholyte. Such a current distribution could accelerate the oxidation (during charging) of the decoupled S-S chains before the complete utilization of the low-order Na_2S_x (x = 8 to 5) in the catholyte.[59,60] This process slowly develops a layer of insulating S at the interface giving rise to high cell resistance. After a while, it hinders the utilization of the catholyte and diminishes the cells' specific capacity, as depicted in Figure 6a.

A similar effect is evident in the HT-NaS cell when the cathodic current collector is in contact with the BASE surface, where insulating S islands on the BASE surface can lead to cracking due to uneven high current density distribution.[61] Adding an electrically insulating layer (viz. alumina fibrous saffil paper) at the interface between the BASE surface and cathodic current collector eliminates this issue.[25] The rise in R_{LF} (charge transfer resistance) after the 21st discharge points out the formation of low-order polysulfides in the catholyte.[18] In Figure 6b, the Raman spectrum shows a change in the higher Raman shift regions, further supporting the formation of lower-order polysulfides in the recovered catholyte after 21 cycles.[37] Besides, the Raman spectrum substantiates that the chemical infrastructure of TEGDME remains unaltered in the recovered catholyte. This finding highlight that reducing the cell operating temperature (125 °C) enhances the catholyte's thermal stability, even though the performance is hindered due to cell configuration.

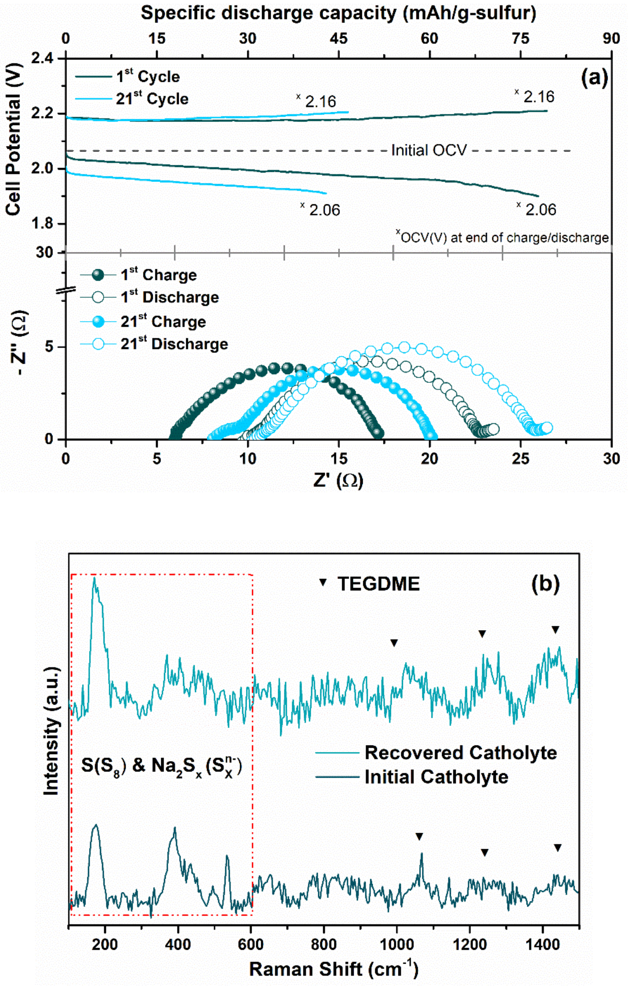

Figure 6. a) Electrochemical measurements of a reconfigured cell with diluted initial catholyte (0.5M Na_2S_5) at 125 °C, **b)** Raman spectrum of the initial and recovered catholyte.

2.6. Effective current distribution at the electrolyte-catholyte interface

Considering the results of section 2.5, to avoid a higher current density distribution at the BASE–catholyte interface than in the bulk of the catholyte, the initial cell configuration is re-instated. The SS mesh around the BASE tube is eliminated, leaving the metallic outer casing of the cell as the cathodic current collector. The outer casing is separated from the BASE surface by 3 mm, rendering the catholyte layer thickness equal to 3 mm (Figure S8). The concentration (0.5M Na_2S_5) and volume (5 ml) of the catholyte in the cell and operating temperature (125 °C) are the same as in Figure 6a. The charge-discharge curves of Figure 7a outline that the cell with a catholyte volume of 5 ml (3 mm) delivers ~10 mAh/g-sulfur higher specific capacity than the cell with SS mesh around the BASE tube (Figure 6a, cycle 1). To further investigate the impact of current density distribution at the BASE surface and cell resistance, the distance between the BASE surface and outer casing is narrowed (Figure S8) to 2 and 1 mm, together with the catholyte volume to 3.3 and 2 ml, respectively. Further reduction in catholyte layer thickness to 1 mm leads to a significant rise (21%) in the specific capacity to 112 mAh/g-sulfur. All cells were electrochemically reversible for 50 cycles, substantiating the notion that avoiding the distribution of a higher current density at the BASE surface than in the bulk of the catholyte can lead to long-term stability.

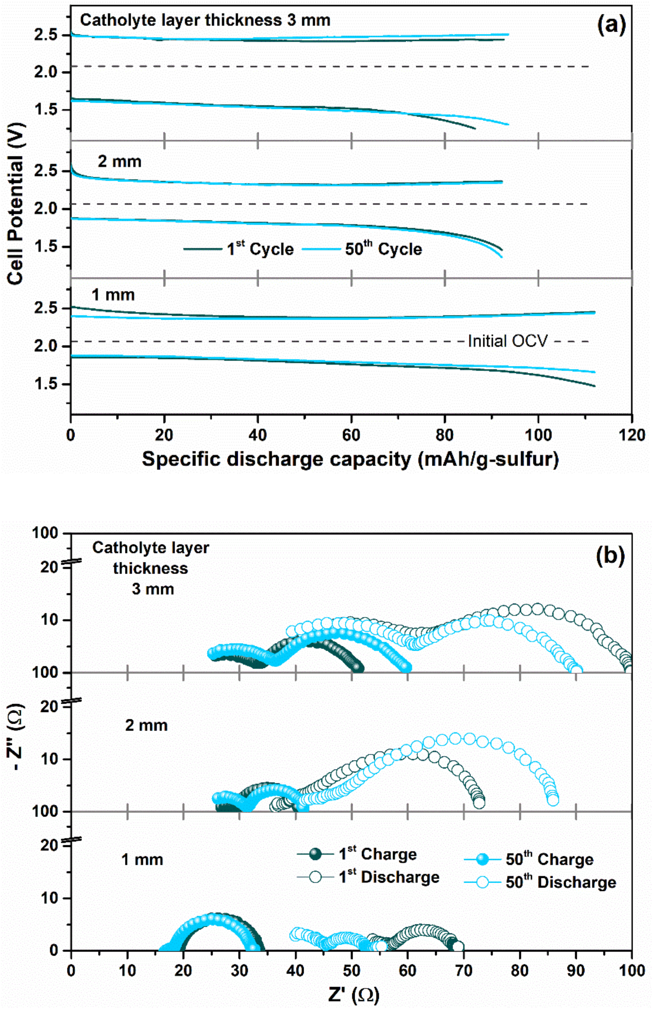

Figure 7. a) Charge-discharge measurement and **b)** EIS measurements for the cells contain initial catholyte (0.5M Na2S5) and operated at 125 °C, but they vary in catholyte layer thickness at BASE-cathodic current collector interface.

EIS spectra of the cells with different thicknesses of the catholyte layer at the end of charge and discharge for 1st and 50th cycles are presented in Figure 7b. The absence of the SS mesh around the BASE tube induces high cell resistance for the cell with the 3 mm thick catholyte layer. The distance of separation between the BASE surface and cathodic current collector (outer casing) increases the effective catholyte layer thickness and diminishes the current density at the BASE interface. The reduction of the catholyte's layer thickness by narrowing the outer cell casing lowers the total cell resistance uniformly, i.e., 3 mm > 2 mm > 1 mm (Table 3). The EIS spectra display two depressed semicircles, where the Z' (x-axis) intercepts of the semicircles dwindle with the reduction in catholyte layer thickness. Here, we postulate that TEGDME traps the Na^+ by forming a crown-like ring with its long ether chain. Consequently, at the BASE-catholyte interface, the Na^+ requests additional activation energy to desolvate from the TEGDME chain before decoupling the S-S chain in the course of the charging process.[62–64] To this end, slicing the catholyte layer's thickness intensifies the current density at the BASE-catholyte interface and diminishes R_{MF}. Successively, this enhancement in the interface favors the effective utilization of the catholyte (its S content) and allows the cell with the minimal catholyte layer thickness (1 mm) to deliver a specific capacity of 112 mAh/g-sulfur.

Table 3. Change in total resistance and OCV, at different states and cycles for the cells with different catholyte layer thickness, contain initial catholyte of 0.5M Na_2S_5 and operated at 125 °C.

Catholyte layer thickness (mm)	Cell cycle	Total resistance $R_{HF} + R_{MF} + R_{LF}$ (Ω)		Open-circuit voltage OCV (V)	
		End of charge	End of discharge	End of charge	End of discharge
3	1	51.25	100.28	2.15	2.06
2		40.86	73.21	2.14	2.06
1		33.47	68.94	2.16	2.05
3	50	57.31	91.38	2.16	2.06
2		41.75	87.53	2.13	2.05
1		32.32	68.94	2.17	2.05

2.7. Hitting the chances to enhance the capacity

Narrowing down the catholyte layer to 1 mm enhanced the current density at the BASE-catholyte interface and improved the catholyte utilization. The molar conductivity (Figure 3) increased with higher Na_2S_5 concentrations in the catholyte until 1M. So, the catholyte (rise in S content) within 0.5 to 1M could further strengthen the current density, on top of the higher volumetric capacity with the same catholyte volume (2 ml). Table 4 presents the volumetric capacity of the cell as a function of more concentrated catholytes (charge-discharge curves are given in Figure S9).[14] The reduction in the cells' specific capacity again pinpoints the ineffective utilization of the catholyte (S content) for higher concentrations.[16] Therefore, the solute solubility in the solvent and phase homogeneity dominates the cell performance as opposed to its transport properties, such as molar conductivity.[56] However, the cells with concentrated catholytes (Figure S9 & S10a) are stable and fully reversible for 50 cycles due to the regulated cut-off limits (predicted alike in Figure 5). The discharge plateau in Figure S9 for the lower concentration (0.6M) shifts marginally to a higher potential in cycle 50 against the initial cycle. Similar behaviour is observed for 0.5M but not yet evidenced for concentrated catholytes.

The total cell resistance ($R_{cell} = R_{HF} + R_{MF} + R_{LF}$) increases as opposed to lower concentration catholytes (Figure S10b & 7b, 1M > 0.75M > 0.6M > 0.5M). Densification of Na_2S_5 (per unit volume) in the catholyte demands additional activation energy to decouple the Na^+, in turn altering the concentration of effective charge carriers and rise in cell resistance.[30,48] For an efficient battery performance estimation (i.e. round-trip energy efficiency), on top of the coulombic efficiency, the voltaic efficiency has an equivalent contribution (detailed in SI, equation S4 – S6). R_{cell} shifts the charge and discharge plateaus away from the OCV and hampers the voltaic efficiencies (from 76 to 65%, 0.5M → 1M, in Table 4).

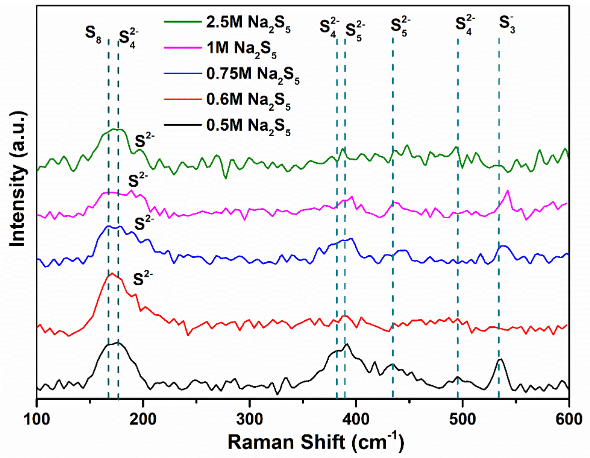

Figure 8. Raman spectrum of initial catholyte with different concentration of Na_2S_5. (broken lines refers to the phases in 0.5M Na_2S_5, as in Figure 2)

Figure 8 displays the Raman spectra of the catholytes with different concentrations of Na_2S_5 (0.5 to 2.5 M). The Na_2S_5 doublet peak (~400 cm^{-1}) diminishes, a broad and intense peak takes its place at ~200 cm^{-1} with an increase in concentration, confirming the formation of low-order Na_2S_x ($x < 5$).[37] On the contrary, in the acquired Raman spectra for 0.5M Na_2S_5 peaks related to lower-order polysulfides beyond Na_2S_4 were not observed. The Na_2S_4 formulated in 0.5M Na_2S_5 is only due to the acid-base equilibrium in the presence of TEGDME, so it confirms the complete chemical dissolution reaction towards the formation of Na_2S_5. The intensity of the peak (534 cm^{-1}) referring to the existence of trisulfide radical (S_3^{*-}) varies with the concentration of Na_2S_5 in TEDME. It is intense at the lower concentration (0.5M) due to the improved solubility of Na_2S_5. Besides, the increase in the content of Na_2S and S exceeds its solubility limit in TEGDME and leads to inhomogeneous Na_2S_5 formation with a variety of low-order polysulfides and unreacted Na_2S (S^{2-}), evidenced in Figure 8.[15] This inhomogeneity in the catholyte generates instability in the chemical equilibrium at the end of charge and discharge, depicted through the variation in the OCV, across the cycles (Figure 9). For the cell with 1M Na_2S_5, both charge and discharge end OCVs are fluctuating. In contrast, the end of charge and discharge OCV for the cells with 0.5M of Na_2S_5 are intact.

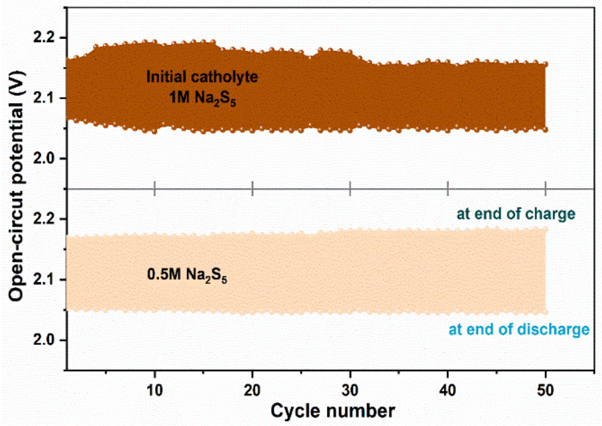

Figure 9. OCV at the end of charge and discharge for cells (1 mm thick layer) operated at 125 °C with different catholyte concentration.

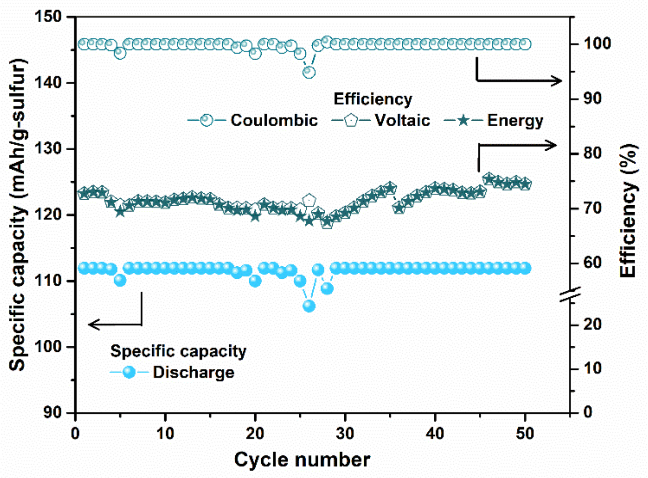

Figure 10. Summary of the long-term performance of the cell operated with 2 ml of 0.5M Na2S5 as initial catholyte (layer thickness 1 mm) at 125 °C. (calculations detailed in SI)

Table 4. Performance summary of the cells with different initial catholyte concentrations operated at 125 °C (given data are for 50th charge-discharge cycle).

Catholyte		Cell capacity		Efficiency		
Na_2S_5 (M)	Layer thickness (mm)	Volumetric (mAh/ml-catholyte)	Specific (mAh/g-sulfur)	Coulombic (%)	Voltaic (%)	Energy (%)
0.5	1	8.2	112	100	76	76
0.6		8.5	89		75	75
0.75		9.5	79		73	73
1		11.8	73		65	65

Further reduction in the initial catholyte concentration (<0.5M) would be more beneficial in terms of solvent-solute dissolution chemistry, but at the expense of capacity due to the reduction in S content. Therefore, 0.5M Na_2S_5 in TEGDME seems to be the appropriate concentration for the initial catholyte. Even though the delivered specific capacity (Figure 10) of the cell with 0.5M Na_2S_5 is 112 mAh/g-sulfur, it represents 90% of the achievable specific capacity of the utilized cycling window ($Na_2S_5 \leftrightarrow Na_2S_8$).[3,55,56] The unutilized 10% stems from the non-active content of S_8 and Na_2S_4 that lies beyond the operational chemical phases. Further, the cell achieved high stability with coulombic efficiency of 97 ± 3% throughout 50 cycles while the catholyte chemical infrastructure shown by the Raman spectra (Figure S12) remained unaltered (Na_2S_5 doublet ~400 cm^{-1} and TEGDME peaks between 1000-1500 cm^{-1}) after 50 deep cycles.

The performance of this IT-NaS cell is superior to other such cells with similar catholyte.[15,16] Lu et.al.,[15] discovered a fade of ~30% in the specific capacity within 30 cycles, the cell operated at 150 °C, and the catholyte contained additive (1M NaI) for effective utilization of low-order polysulfides. Herein, we managed to boost performance at a record-low operating temperature (125 °C) for an IT-NaS battery system, and at the same time, improve the cycle life.

3. Conclusion

The execution of optimized operational strategies boosted markedly the cell's stability and long-term performance. The main changes involved are diluted catholyte concentration, narrowed catholyte layer, and reduction in practical cycling limits. We realized a cell with an initial catholyte of 0.5M Na_2S_5 capable of delivering 90% of its achievable specific capacity for 50 cycles. The coulombic efficiency lingered at > 97 ± 3%, and an average total cell energy efficiency of 73 ± 4% was obtained. The dissolution limit of Na_2S_x and preventing the phase segregation of S_8 in the catholyte are paramount in achieving long-term performance. Apart from the stability and enhancement in long-term performance, we ran for the first time the IT-NaS system at a low operating temperature (125 °C).

The agenda for further research entails i) tuning of the catholyte chemical solubility for low-order polysulfide to utilize Na_2S_3, ii) enhancing the performance further by boosting the specific capacity and iii) introducing a flowable catholyte to enhance the volumetric discharge capacity of the cell. Accordingly, the achievable theoretical capacity for extending the charge-discharge cycling limit to ($Na_2S_3 \leftrightarrow Na_2S_8$) will rise to 350 mAh/g-sulfur (or at least 209 mAh/g-sulfur for exploring $Na_2S_4 \leftrightarrow Na_2S_8$)[3,55,56] and would be comparable to HT-NaS cells (utilizes $Na_2S_3 \leftrightarrow S$).[3]

4. Experimental Section

Catholyte preparation: High purity sulfur (S metals basis, 99.9995%) and sodium sulfide (Na_2S anhydrous, 96.07%) were purchased from Alfa Aesar and used as received. The organic solvent tetraethylene glycol dimethyl ether (TEGDME) was bought from Acros Organics with <0.05% of water. It was further dried by using the pre-activated molecular sieves beats (4Å, Alfa Aesar) and filtered through a class 597 Whatman filter paper. The catholyte was formulated by adding the calculated amount of Na_2S and S to TEGDME solvent to meet the required stoichiometry (e.g., 0.5M $Na_2S_5 \rightarrow$ 0.5M Na_2S + 2M S). For homogeneous mixing, it was continuously stirred (rpm = 500) at 125 °C for 8 h. The preparation of the catholyte and cell fabrication for both battery and conductivity measurements was conducted in an argon-filled glove box (Inert Corporation) maintained within O_2 and H_2O concentrations of 0.1 and 0.5 ppm, respectively.

Cell set-up for galvanostatic charge-discharge and conductivity measurements: Our lab-scale battery cells consist of two tubular compartments (anode and cathode). The inner and central compartment is a beta-alumina solid electrolyte (BASE) tube with an active surface area of ~3 cm^2, purchased from Ionotec, UK. An appropriately in-house machined SS graded 316 outer compartment serves as the cathodic side and outer casing simultaneously. A SS screw cap was used as an air-tight closer (Figure S1a), to which the central BASE tube was fixed by a high-temperature resist two-component epoxy (JB weld 8265S cold weld). The BASE was purchased in a pre-sealed condition with a lead to serve as the anodic terminal, and the tube wall acts as a Na^+ conducting separator between the anode and cathode. Before using, the BASE tubes were heated to 300 °C for 6 h in a muffle furnace. A nickel strip welded to the outer casing of the cell was used as the cathodic current collector. In some cases, an SS mesh (50% porous) was wound around the central BASE tube to serve as the cathodic current collector, probed by a tungsten wire (0.5 mm thick).

The catholyte's electrical conductivity was determined by an in-house made borosilicate glass conductance cell with two symmetrical gold (wire 0.5 mm thick) electrodes, sealed by an air-tight Teflon stopper (Figure S1b). To establish a precise current path between the electrodes, less than 2 mm of the gold wire was exposed to the catholyte. Prior to each measurement, the geometrical cell constant of the conductance cell was determined by using the conductivity calibration standards (HANNA instruments 12.88 mS/cm and 1413 µS/cm) at room temperature. The cell components were washed thoroughly in deionized water and ethanol under ultrasonic agitation and dried overnight in a hot air oven at 120 °C. The conductance cell was filled with 7 ml of catholyte or conductivity calibration standards. In both cells (battery and conductance cells), a stirrer bar (VWR, a diameter of 10, 8, or 6 mm depending on the inner diameter of the catholyte compartment) was employed to create convection to the catholyte. The assembled cells were hermetically sealed and brought out of the glove box for testing. At that time, they were heated to the desired operating temperature (125 or 150 °C) in a silicon oil bath (Sigma Aldrich) over a hot plate stirrer (Velp Scientifica AM4).

Electrochemical measurements: An IVIUMnSTAT potentiostat (Ivium technologies) was used to perform electrochemical measurements. Before conducting the electrochemical measurements, all the battery cells were subjected to an initial conditioning process to establish a uniform temperature distribution throughout the cell and better wettability at the BASE interfaces. It entails the aging of the cells at its operating temperature for 24 h, followed by two slow charge-discharge cycles at low current densities (± 0.3 and ± 1.2 mA/cm^2 normalized by the active surface area of BASE).[14,15] Meanwhile, the agitation of the catholyte was gradually increased to 600 rpm. Next, they were set to galvanostatic charge-discharge measurements at the current density of ± 2.5 mA/cm^2 with potential (V) and time (sec) cut-off limits. At the end of every charge and discharge step, the cell was set to rest (zero current) for 5 min, and then an open-circuit voltage (OCV) was recorded. The short rest before the OCV diminishes any voltage drift and allows the battery to reach chemical equilibrium. The electrochemical impedance spectrum (EIS) was recorded after every 5th charge and discharge, with 5 min of rest before and after the EIS measurements. To avoid drift in the cell potential, EIS spectra were recorded at a constant current mode between 250 kHz - 0.1 Hz.[65,66] The applied constant current was 10% of its respective galvanostatic charge-discharge current. In the case of the conductance cell, EIS spectrums were recorded at constant potential mode by applying a small sinusoidal voltage (10 mV) at frequencies between 250 kHz and 1 Hz. The conductance cells were held at the desired measurement temperature for 2 h to establish the homogeneous temperature distribution while the catholyte was stirred at 600 rpm. The stirrer was turned off 15 min before the EIS measurements. The reported conductivity was an average of the three EIS recordings, taken at 15 min intervals in-between.

Analysis of the catholyte's chemical infrastructure: The battery cells were moved to the glove box after the galvanostatic charge-discharge measurements to recover the catholyte. Selected recovered and fresh catholytes were analyzed through Raman spectroscopy (Avantes AvaRaman-532 TEC with 532 nm laser). Sampling details are provided in the SI (supporting information, Figure S13). For each sample, triplicate Raman spectra were recorded for reproducibility. The spectrum measurement and processing were performed by using AvaSoft8 software provided by Avantes. Further analyses such as peak identification and fitting were done in Originlab®.

Acknowledgements

The authors gratefully acknowledge the Ministry of Economic Affairs of the Netherlands for financing the research project "NaSTOR residential energy system storage prototype (NaSTOR prototype)" project no. TEUE116130 under the program line "TKI urban energy – Topsector Energy (TSE)". S.K thanks the members from Nouryon R&D center, NL and Ionotec, UK (industrial partners of another collaborative project TEUE518006) for their extended support and useful discussions on this work. S.K and M.N.T are thankful to E. Langereis for input on the graphical abstract.

[1] I. Hasa, S. Mariyappan, D. Saurel, P. Adelhelm, A. Y. Koposov, C. Masquelier, L. Croguennec, M. Casas-Cabanas, *J. Power Sources* **2021**, *482*, 228872.
[2] R. Fang, J. Xu, D. W. Wang, *Energy Environ. Sci.* **2020**, *13*, 432–471.
[3] L. Medenbach, P. Adelhelm, *Top. Curr. Chem.* **2017**, *375*, 1–25.
[4] P. Adelhelm, P. Hartmann, C. L. Bender, M. Busche, C. Eufinger, J. Janek, *Beilstein J. Nanotechnol.* **2015**, *6*, 1016–1055.
[5] "World's Largest Battery in Abu Dhabi – 108 MW/648 MWh | DeepResource," can be found under https://deepresource.wordpress.com/2019/02/05/worlds-largest-battery-in-abu-dhabi-108-mw-648-mwh/, **n.d.**
[6] K. B. Hueso, M. Armand, T. Rojo, *Energy Environ. Sci.* **2013**, *6*, 734–749.
[7] S. H. Chung, A. Manthiram, *Adv. Mater.* **2019**, *31*, 1901125.
[8] A. Manthiram, X. Yu, *Small* **2015**, *11*, 2108–2114.
[9] I. Kim, J. Y. Park, C. H. Kim, J. W. Park, J. P. Ahn, J. H. Ahn, K. W. Kim, H. J. Ahn, *J. Power Sources* **2016**, *301*, 332–337.
[10] Z. Wen, Y. Hu, X. Wu, J. Han, Z. Gu, *Adv. Funct. Mater.* **2013**, *23*, 1005–1018.
[11] "Ionotec - beta alumina supplier-Conductive ceramics - beta alumina," can be found under http://www.ionotec.com/conductive-ceramics.html, **n.d.**
[12] H. Ryu, T. Kim, K. Kim, J. H. Ahn, T. Nam, G. Wang, H. J. Ahn, *J. Power Sources* **2011**, *196*, 5186–5190.
[13] G. Nikiforidis, M. C. M. Van de Sanden, M. N. Tsampas, *RSC Adv.* **2019**, *9*, 5649–5673.
[14] G. Nikiforidis, G. J. Jongerden, E. F. Jongerden, M. C. M. van de Sanden, M. N. Tsampas, *J. Electrochem. Soc.* **2019**, *166*, A135–A142.
[15] X. Lu, B. W. Kirby, W. Xu, G. Li, J. Y. Kim, J. P. Lemmon, V. L. Sprenkle, Z. Yang, *Energy Environ. Sci.* **2013**, *6*, 299–306.
[16] F. Yang, S. M. A. Mousavie, T. K. Oh, T. Yang, Y. Lu, C. Farley, R. J. Bodnar, L. Niu, R. Qiao, Z. Li, *Adv. Energy Mater.* **2018**, *8*, 1701991.
[17] K. M. Abraham, R. D. Rauh, S. B. Brummer, *Electrochim. Acta* **1978**, *23*, 501–507.
[18] Y. Wang, D. Zhou, V. Palomares, D. Shanmukaraj, B. Sun, X. Tang, C. Wang, M. Armand, T. Rojo, G. Wang, *Energy Environ. Sci.* **2020**, *13*, 3848–3879.
[19] P. J. Binden, Binden, P. J., *STIN* **1993**, *94*, 19035.
[20] Y. Jung, S. Kim, B. S. Kim, D. H. Han, S. M. Park, J. Kwak, *Int. J. Electrochem. Sci.* **2008**, *3*, 566–577.
[21] "Large Energy Storage Systems Handbook - F. Barnes, J. Levine (CRC, 2011) BBS.pdf," can be found under https://www.routledge.com/Large-Energy-Storage-Systems-Handbook/Barnes-Levine/p/book/9781138071964, **n.d.**
[22] Z. F. Hussien, L. W. Cheung, M. F. M. Siam, A. B. Ismail, *Elektrika* **2007**, *9*, 66–72.
[23] L. W. Chung, M. F. M. Siam, A. B. Ismail, Z. F. Hussien, in *Natl. Power Energy Conf. PECon 2004 - Proc.*, **2004**, pp. 205–210.
[24] P. J. Johnson, *J. Power Sources* **1990**, *32*, 63–70.
[25] P. J. Johnson, A. A. Koenig, *J. Electrochem. Soc.* **1990**, *137*, 1121–1125.
[26] A. Gupta, A. Bhargav, A. Manthiram, *Adv. Energy Mater.* **2019**, *9*, 1803096.
[27] K. Ueno, R. Tatara, S. Tsuzuki, S. Saito, H. Doi, K. Yoshida, T. Mandai, M. Matsugami, Y. Umebayashi, K. Dokko, M. Watanabe, *Phys. Chem. Chem. Phys.* **2015**, *17*, 8248–8257.
[28] Q. He, Y. Gorlin, M. U. M. Patel, H. A. Gasteiger, Y. C. Lu, *J. Electrochem. Soc.* **2018**, *165*, A4027–A4033.
[29] S. M. Blair, E. C. Kempen, J. S. Brodbelt, *J. Am. Soc. Mass Spectrom.* **1998**, *9*, 1049–1059.
[30] F. Y. Fan, M. S. Pan, K. C. Lau, R. S. Assary, W. H. Woodford, L. A. Curtiss, W. C. Carter, Y. M. Chiang, *J. Electrochem. Soc.* **2016**, *163*, A3111–A3116.
[31] S. Tsuzuki, T. Mandai, S. Suzuki, W. Shinoda, T. Nakamura, T. Morishita, K. Ueno, S. Seki, Y. Umebayashi, K. Dokko, M. Watanabe, *Phys. Chem. Chem. Phys.* **2017**, *19*, 18262–18272.
[32] N. Angulakshmi, A. M. Stephan, *Front. Energy Res.* **2015**, *3*, 17.
[33] Y. C. Lu, Q. He, H. A. Gasteiger, *J. Phys. Chem. C* **2014**, *118*, 5733–5741.
[34] H. Cheng, P. Wang, J. Luo, J. Fransaer, D. E. De Vos, Z. H. Luo, *Ind. Eng. Chem. Res.* **2015**, *54*, 3107–3115.
[35] D. Zheng, G. Wang, D. Liu, J. Si, T. Ding, D. Qu, X. Yang, D. Qu, *Adv. Mater. Technol.* **2018**, *3*, 1700233.
[36] J. H. Gordon, J. J. Watkins, *Sodium-Sulfur Battery with a Substantially Non-Porous Membrane and Enhanced Cathode Utilization*, **2010**.
[37] M. Hagen, P. Schiffels, M. Hammer, S. Dörfler, J. Tübke, M. J. Hoffmann, H. Althues, S. Kaskel, *J. Electrochem. Soc.* **2013**, *160*, A1205–A1214.
[38] O. El Jaroudi, E. Picquenard, N. Gobeltz, A. Demortier, J. Corset, *Inorg. Chem.* **1999**, *38*, 2917–2923.
[39] G. J. Janz, J. R. Downey, E. Roduner, G. J. Wasilczyk, J. W. Coutts, A. Eluard, *Inorg. Chem.* **1976**, *15*, 1759–1763.
[40] J. T. Yeon, J. Y. Jang, J. G. Han, J. Cho, K. T. Lee, N. S. Choi, *J. Electrochem. Soc.* **2012**, *159*, A1308–A1314.
[41] H. L. Wu, L. A. Huff, A. A. Gewirth, *ACS Appl. Mater. Interfaces* **2015**, *7*, 1709–1719.
[42] R. Steudel, Y. Steudel, *Chem. - A Eur. J.* **2013**, *19*, 3162–3176.
[43] M. Kartal, A. Alp, H. Akbulut, *Acta Phys. Pol. A* **2016**, *129*, 816–818.
[44] S. Kandhasamy, Molten Carbonate Electrolyte Based Thermocells for High Temperature Waste Heat Recovery, Norwegian University of Science and Technology, **2019**.
[45] N. K. Goh, L. S. Chia, *Singapore J. Educ.* **1980**, *3*, 27–31.
[46] W. Zhang, X. Chen, Y. Wang, L. Wu, Y. Hu, *ACS Omega* **2020**, *5*, 22465–22474.
[47] G. Horwitz, C. Rodríguez, M. Factorovich, H. R. Corti, *J. Phys. Chem. C* **2019**, *123*, 12081–12087.
[48] J. P. Southall, H. V. S. A. Hubbard, S. F. Johnston, V. Rogers, G. R. Davies, J. E. McIntyre, I. M. Ward, *Solid State Ionics* **1996**, *85*, 51–60.
[49] S. Seki, K. Hayamizu, S. Tsuzuki, K. Takahashi, Y. Ishino, M. Kato, E. Nozaki, H. Watanabe, Y. Umebayashi, *J. Electrochem. Soc.* **2018**, *165*, A542–A546.
[50] X. Lu, J. P. Lemmon, V. Sprenkle, Z. Yang, *Jom* **2010**, *62*, 31–36.
[51] M. C. H. McKubre, F. L. Tanzella, S. I. Smedley, *J. Electrochem. Soc.* **1989**, *136*, 303–305.
[52] U. Westerhoff, K. Kurbach, F. Lienesch, M. Kurrat, *Energy Technol.* **2016**, *4*, 1620–1630.
[53] X. Qiu, Q. Hua, L. Zheng, Z. Dai, *RSC Adv.* **2020**, *10*, 5283–5293.
[54] M. Wang, J. Newman, *J. Electrochem. Soc.* **1995**, *142*, 761–764.
[55] X. Yu, A. Manthiram, *J. Phys. Chem. Lett.* **2014**, *5*, 1943–1947.

[56] I. Kim, J. Y. Park, C. Kim, J. W. Park, J. P. Ahn, J. H. Ahn, K. W. Kim, H. J. Ahn, *J. Electrochem. Soc.* **2016**, *163*, A611–A616.

[57] S. S. Zhang, K. Xu, T. R. Jow, *Electrochim. Acta* **2006**, *51*, 1636–1640.

[58] K. Sathiyaraj, G. D. Bhuvaneswari, N. Kalaiselvi, A. J. Peter, *IEEE Trans. Nanotechnol.* **2012**, *11*, 314–320.

[59] B. R. Karas, *J. Electrochem. Soc.* **1985**, *132*, 1261–1266.

[60] B. R. Karas, R. N. King, *J. Electrochem. Soc.* **1985**, *132*, 1266–1272.

[61] N. K. Gupta, G. J. Tennenhouse, in *Proc. - Electrochem. Soc.*, Electrochem Soc Inc, **1979**, pp. 446–456.

[62] F. Sagane, T. Abe, Z. Ogumi, *J. Power Sources* **2010**, *195*, 7466–7470.

[63] F. Sagane, T. Abe, Y. Iriyama, Z. Ogumi, *J. Power Sources* **2005**, *146*, 749–752.

[64] M. Busche, T. Leichtweiss, C. Fiedler, T. Drossel, M. Geiss, M. Wei, A. Kronenberger, D. Weber, J. Janek, *Adv. Mater. Interfaces* **2020**, *7*, 2000380.

[65] Y. Fernández Pulido, C. Blanco, D. Anseán, V. M. García, F. Ferrero, M. Valledor, *Meas. J. Int. Meas. Confed.* **2017**, *106*, 1–11.

[66] Gamry Instruments, “EIS - Potentiostatic or Galvanostatic Mode,” **2017**.

Graphical Abstract

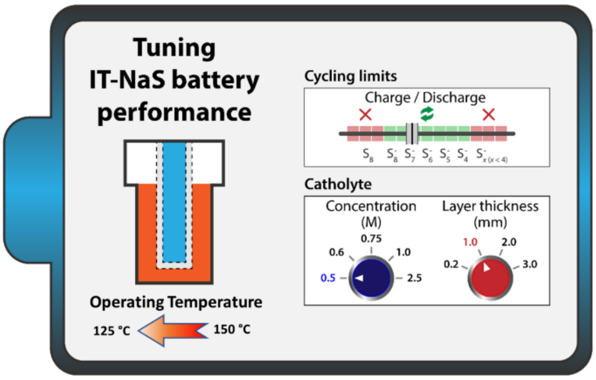

Established an intermediate temperature NaS battery with a tubular Na-β″ alumina solid-state electrolyte and for the first time operated the system at a low temperature of 125 °C. Here the catholyte is a mixture of organic solvent (TEGDME), solvated S, and Na_2S. Catholyte's concentration and layer thickness are accessed to improve the cell performance. Besides, the cut-off limit for charge-discharge cycling is regulated for long-term stability.

<u>**Supporting Information**</u>

Operational strategies to improve the performance and long-term cyclability of intermediate temperature sodium-sulfur (IT-NaS) battery

Sathiyaraj Kandhasamy[1,*], Georgios Nikiforidis[2,3], Gert Jan Jongerden[4], Ferdy Jongerden[4], Mauritius C. M. van de Sanden[1,5], and Mihalis N. Tsampas[1,*]

[1]*Dutch Institute for Fundamental Energy Research (DIFFER), The Netherlands*
[2]*Laboratory of Physico-Chemistry of Materials and Electrolytes for Energy, University of Tours, France*
[3]*LE STUDIUM Institute for Advanced Studies, France*
[4]*Exergy Storage Components and Systems, The Netherlands*
[5]*Department of Applied Physics, Eindhoven University of Technology, The Netherlands*
* *Corresponding authors E-mail:* S.Kandhasamy@differ.nl (S.K); M.Tsampas@differ.nl (M.N.T)

Cells set-up

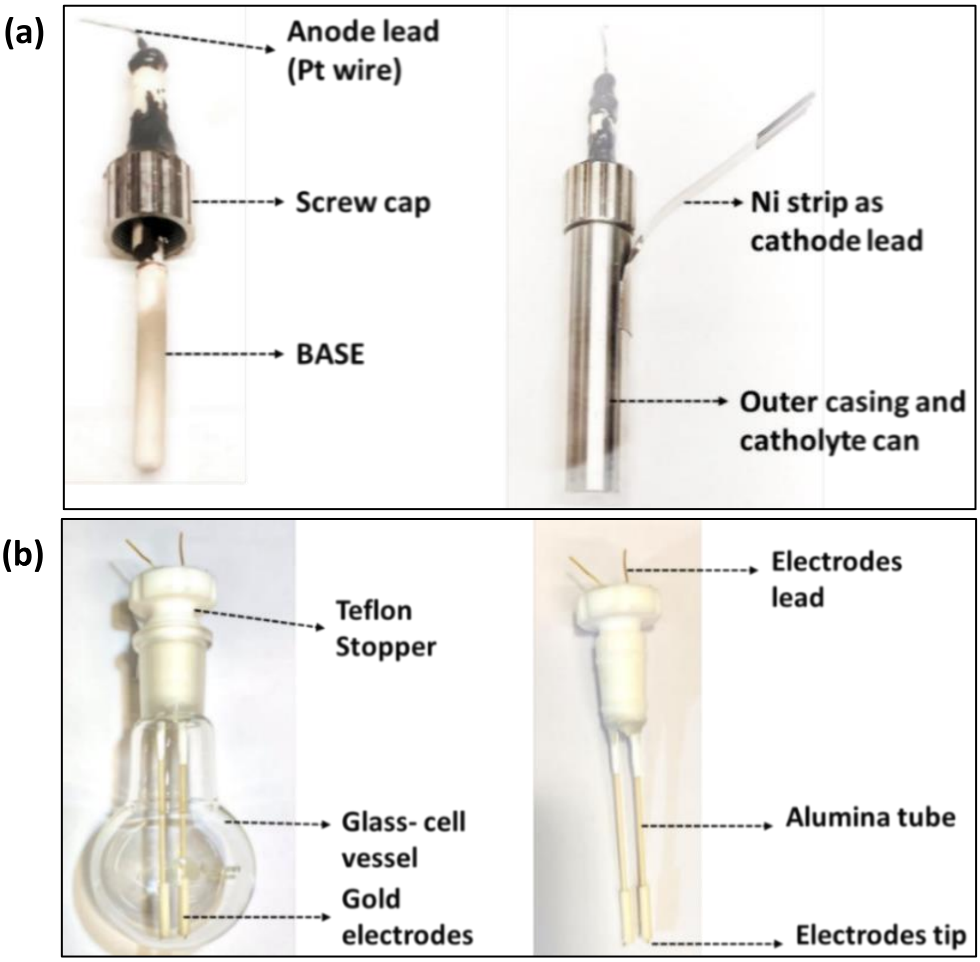

Figure S1. a) Central compartment BASE tube fixed to the SS screw cap (right) and as-assembled IT-NaS lab cell (left). **b)** Conductance cell (right) used for conductivity measurement and its symmetrical gold electrodes (left).

Cell components contribution to ohmic resistance

Each component of the cell contributes (Figure S4) to the cell's resistance. The ohmic resistance (i.e., R_{HF}, the x-axis intercept at the higher frequency) is described by the following equation.

$$R_{HF} = R_A + R_{AC} + R_{BASE} + R_{Catholyte} + R_{CC} + R_C \qquad (S1)$$

Where,

R_A: Resistance of anode lead (resistivity of Pt = 10.6×10^{-8} Ω·m @ RT)

R_{AC}: Resistance of anodic current collector (resistivity of carbon felt <4×10^{-3} Ω·m @ RT)

R_{BASE}: Resistance of BASE (Na^+ resistivity in BASE @ 100 and 200 °C is 0.6 and 0.1 Ω·m, respectively)

$R_{catholyte}$: Resistance of 0.5M Na_2S_5 (resistivity of 10 Ω·m, measured conductivity @ 125 °C is 1 ± 0.05 mS/cm)

R_{AC}: Resistance of SS 316 (resistivity @ RT is 6.9×10^{-7} Ω·m)

R_A: Resistance of Ni strip (resistivity @ RT is 6.9×10^{-8} Ω·m)

As an indication, the values for R_A, R_{AC}, R_{CC}, R_C at RT are given.

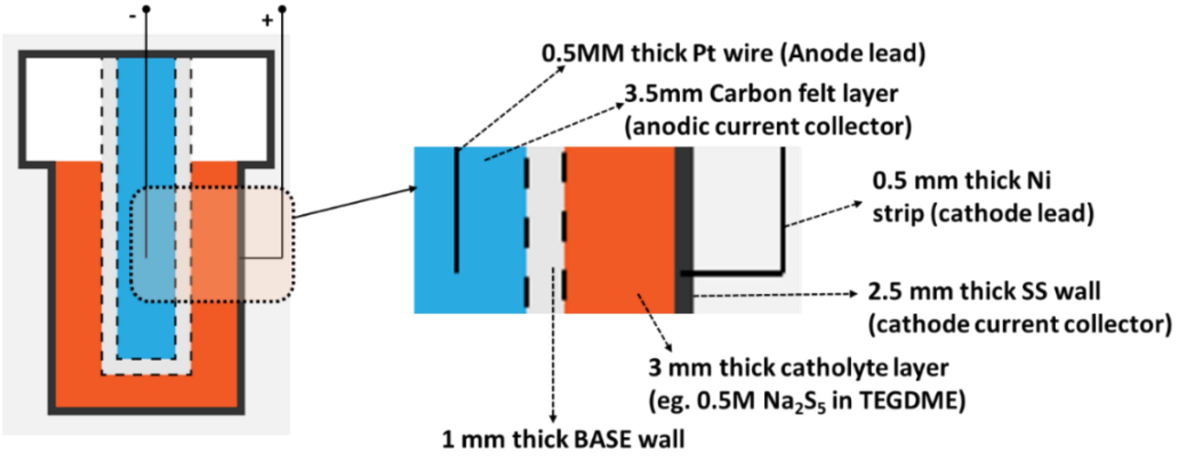

Figure S2. Cells components that contribute to ohmic resistance (R_{HF}).

Change in catholyte's chemical infrastructure of the cell used for Figure 1

The Raman spectra (fingerprint region for the S and Na_2S_x) of the as-prepared and recovered catholytes (2.5M Na_2S_5) from the cell used in Figure 1 are shown in Figure S3a. They reveal that the polysulfide compositions of the recovered catholyte are distinct from the as-prepared. Along with the broad peak (350-500 cm^{-1}) denoting the Na_2S_4 and Na_2S_5 phase, the peak at ~175 cm^{-1} is intensified in the recovered catholyte. Fitting peaks to the spectrum

(Figure S3b) display that the insulating S (i.e., S_8) phase has a substantial contribution for the peak (~175 cm^{-1}) than the desired polysulfide phase. Hence, the formation of S in the recovered catholyte due to deeper charging state on cycle-A signifies the occurrence of permanent, irreversible loss of active (S) species even before cycle-B.

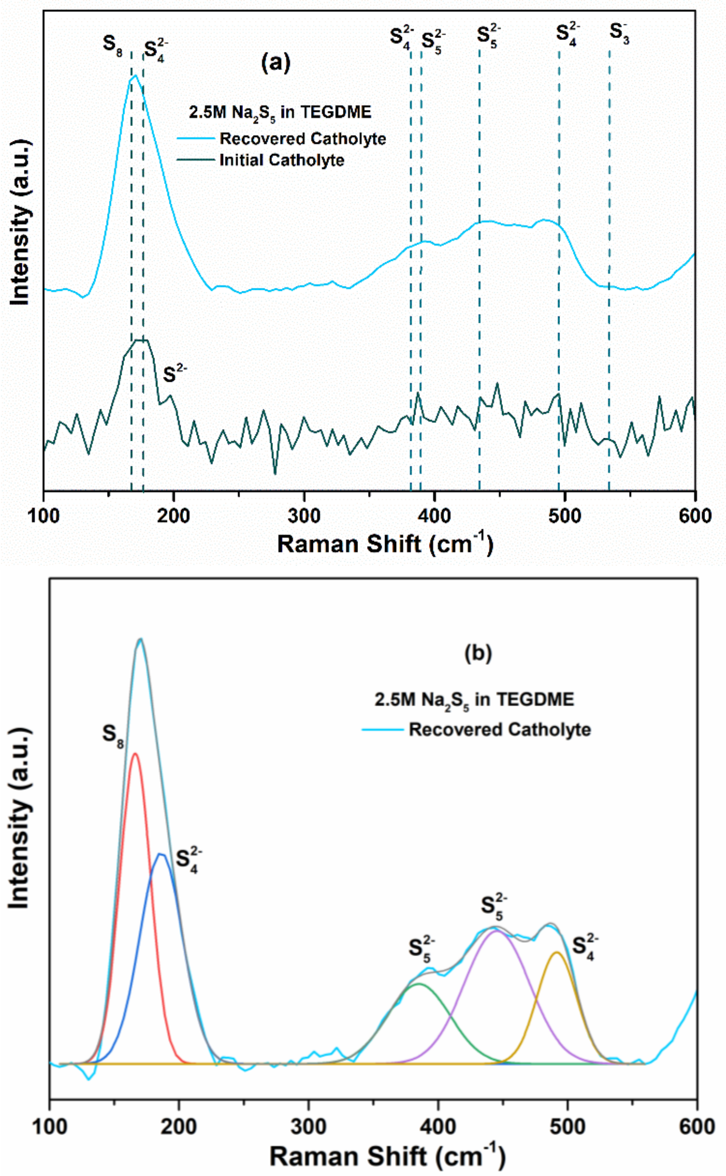

Figure S3. a) Raman spectrum of initial and recovered (after cycle-B in Figure 1) catholyte (2.5M Na_2S_5) of the cell with SS mesh around the BASE and operated at 150 °C, **b)** recovered catholyte's spectrum fitted with peaks for additional details.

EIS spectrum analysis

The recorded EIS spectra were analyzed by fitting the equivalent circuits below to delineate the values for the individual resistance components.

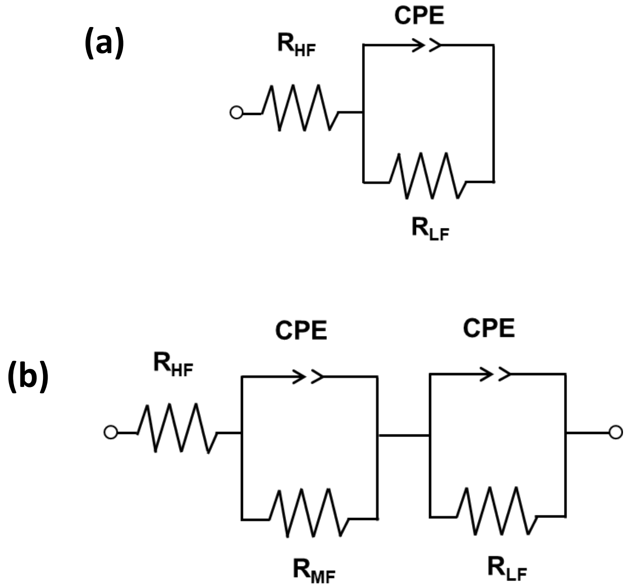

Figure S4. Equivalent circuits used to analyze single semicircle EIS spectra (**a)** with two resistance components), **b)** EIS spectra with an additional semicircle (right, three resistance components). *(R – resistances & CPE – constant phase element)*

Molecular model for solvent-solute interaction in the catholyte mixture

The catholyte's solvent of interest tetraethylene glycol dimethyl ether (TEGDME) possesses a long-chain of ethers coordinated with five periodic binding sites (i.e., oxygen) with donor nature. Thebinding sites of each TEGDME molecule enforce a strong solvent-solute interaction to cage a single Na^+ from solvated sodium polysulfides (Na_2S_x). An online molecular modeling tool, "MolView" was used to visualize (Figure S2) the possible solvent-solute interactions that could be formulated in the catholyte mixture. Figure S2 shows the energy equilibrated (after 5 × 100 iterations of energy minimization steps) 3D model of the individual molecules and the molecular complexes of the catholyte mixture. The five oxygen-binding sites of the TEGDME enforce a strong solvent-solute interaction with a single Na^+ to frame an open-ended crown (Figure S2c), consistent with the literature.[31] In addition, we extended the approximation to model the interaction of a single Na_2S_5 solvated molecule with TEGDME solvent in 0.5M Na_2S_5, as illustrated in figure S2d.

Tsuzuki, et al.,[31] modeled an identical $[Na(TEGDME)]^+$ complex to that of figure S2c, and by using the Gaussian 09 program and found the stabilization energy for this complex formation to be ca. -77.1 kcal mol^{-1}. The stabilization energies decrease with the reduction in chain length of the glyme (i.e. reduction oxygen sites).

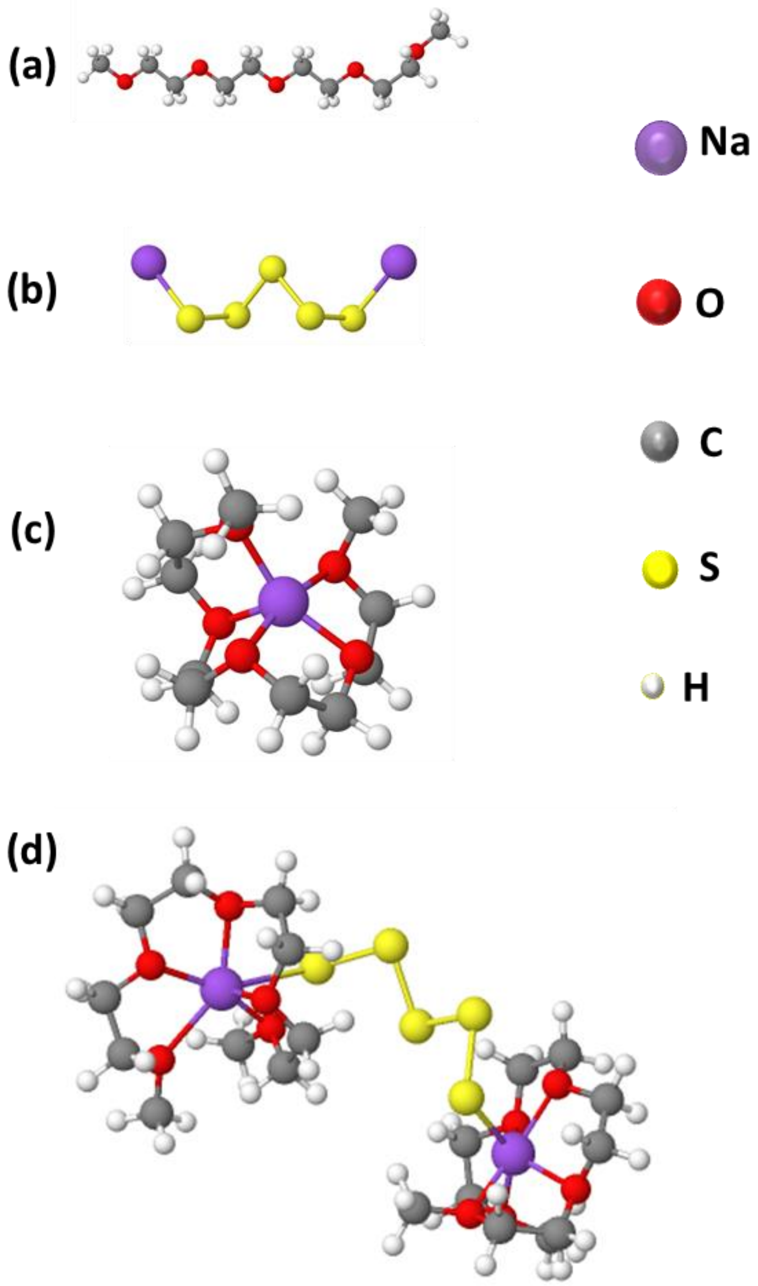

Figure S5. Molecular characterization of the IT-NaS catholyte components. **a)** Solvent tetraethylene glycol dimethyl ether (TEGDME), **b)** solute sodium polysulfide (Na_2S_5), **c)** An open-ended crown by TEGDME to cage a single Na^+, and **d)** Initial catholyte (0.5M Na_2S_5) solvent-solute interaction between TEGDME and Na_2S_5.

Table S1. Stabilization energies for the formation of $[Na(glyme)]^+$ complexes.[31]

Glyme solvent	Tetraglyme (TEGDME)	Triglyme	Diglyme	Monoglyme
Oxygen sites	5	4	3	2
Stabilization energy (Kcal mol^{-1}) for complex formation with Na^+				
Chain length	Decreases →			

Determination of electrical conductivity of the catholytes

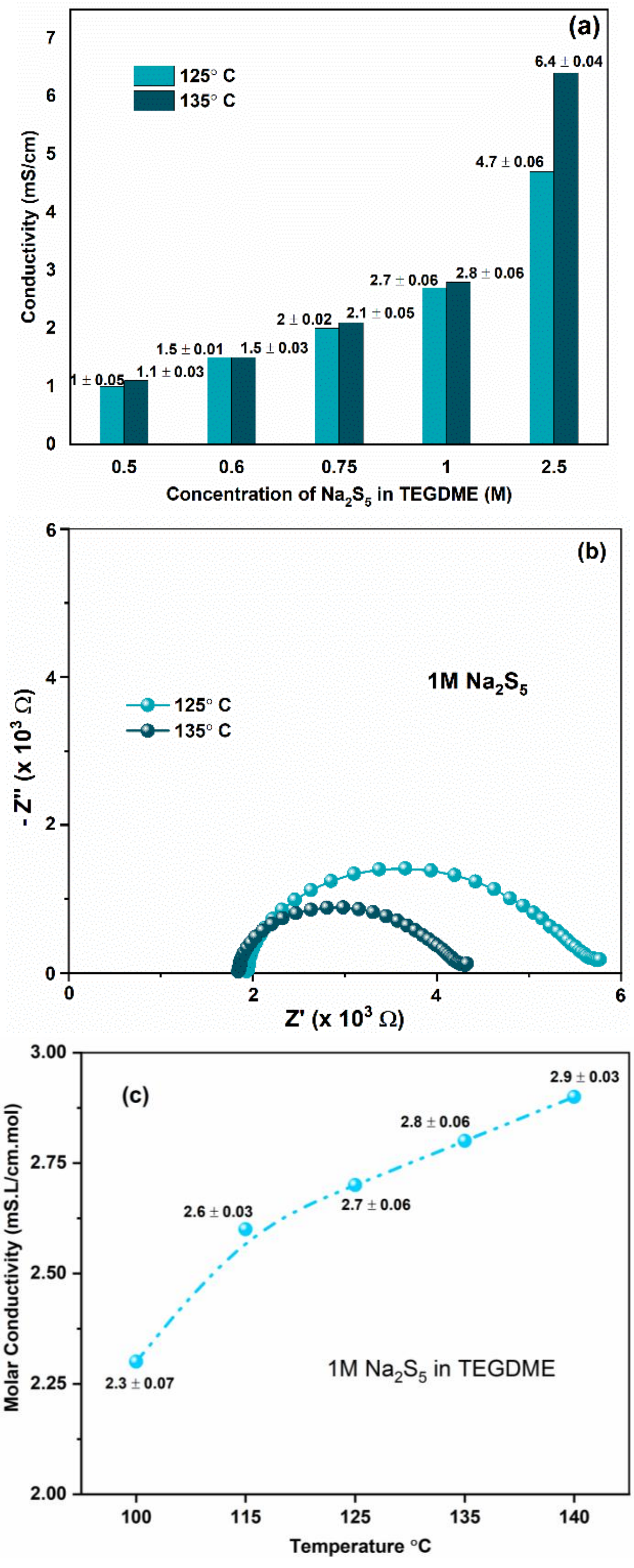

Figure S6. a) Conductivity of the as-prepared catholytes with different concentrations of Na_2S_5 in TEGDME. **b)** Conductance cell measurements, EIS spectra of 1M Na_2S_5, R_S is the x-axis intercept at a higher frequency. **c)** The molar conductivity of the as-prepared 1M Na_2S_5 catholyte at different temperatures.

The R_S (x-axis intercept at a higher frequency) from the EIS measurements were used to determine the electrical conductivity (σ) of the catholyte mixture by the following relationship,[40]

$$\sigma\ (\mathrm{mS/cm}) = \frac{1}{R_S}\left(\frac{l}{A}\right) \qquad \text{(S2)}$$

Here, l reflects the distance between the electrodes, and A describes the cross-sectional area of the current path. This ratio $\left(\frac{l}{A}\right)$ is defined as the cell constant (it is 5.31 $\mathrm{cm^{-1}}$ for the cell used in Figure S6b).

For refining the practical operating temperature, we considered the melting point of sulfur (115 °C) and the flashpoint of TEGDME (141 °C) as the minimum and maximum threshold limits, to accomplish effective reactivity of sulfur and TEGDME's thermal stability. To ensure that the cell lies within these thresholds, we selected 125 and 135 °C. However, Figure S6c presented the molar conductivity of 1M Na_2S_5 (benchmarked catholyte concentration upper limit), where no significant variation was evident between 100 and 140 °C. The result of Figure S6c suggests that for the catholytes at low concentrations (i.e., < 1M), the molar conductivity shouldn't possess considerable transformation, which is also true from the data obtained at the temperature of interest (125 & 135 °C). Thus, the molar conductivity is not intended to measure at the other temperatures within the given range for the catholytes at low concentrations.

Measurement to determine the desired cut-off limit for charge-discharge cycling

For Figure 5 in session 2.4, the EIS and OCV data are collected at several intermediate stages during the galvanostatic charge-discharge cycles at ± 2.5 $\mathrm{mA/cm^2}$. At the initial state (C_0), OCV and EIS are recorded before heading to stage C_1 through a 45 min charging step. Reaching C_1, the cell rests (i.e., zero current) for 5 min, followed by an EIS measurement and another 5-minute rest before moving to the next charging step. The intermediate states C_1 to C_3 are extended via a 45 min charging step. Then, to adjust the charging cut-off limit when approaching the full charge state (C_4 & C_5), the charging steps are shortened to 15 min. Faraday's law determines this timeline by taking into account the appropriate content of Na^+ for the electrochemical conversion of Na_2S_5 to Na_2S_8.

The mathematical form of Faraday's first law of electrolysis is given by,

$$\mathrm{m} \times \alpha \times \mathrm{Q} \qquad \text{(S3)}$$

Where,

m: the mass of the substance liberated at the electrode (here it is Na from cathode),

Q: the quantity of electricity (charge) passed through the electrodes (current I x time t).

Equation (S3) can be rewritten as,

$$m = \left(\frac{E}{96{,}485}\right) \times Q \tag{S4}$$

$$m = \left(\frac{E}{96{,}485}\right) \times (I \times t) \tag{S5}$$

Where,

$\left(\frac{E}{96{,}485}\right)$ - the proportionality constant (electrochemical equivalent),

E - the equivalent weight of the substance liberated (Na = 23 g/mol).

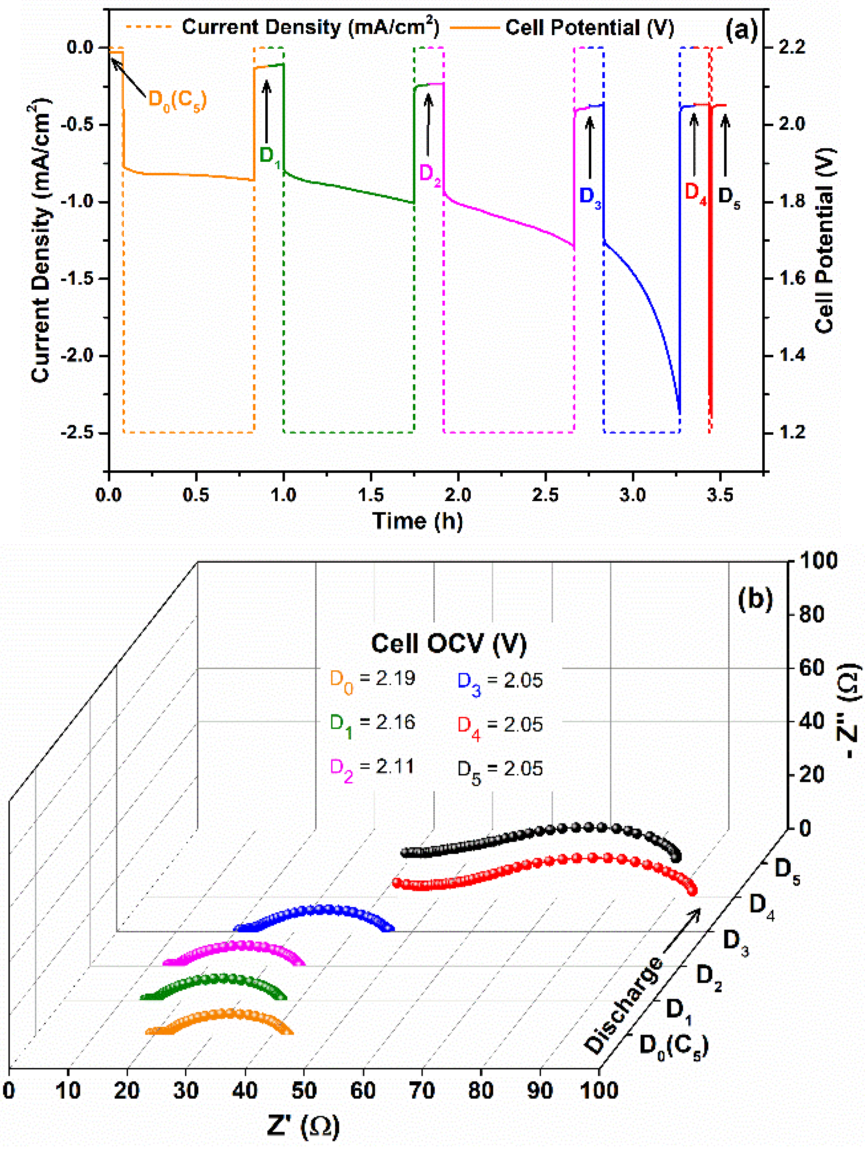

Figure S7. EIS at various intermediate stages on electrochemical discharge for a cell with diluted catholyte operated at 125 °C. **a)** Galvanostatic discharge voltage profile and **b)** EIS spectra.

In our case, the known quantities are (m, E, I), so by using these values (t), the timeline for the measurements in Figures 5 & S6 can be evaluated. For example, a cell with 2 ml of 0.5M Na_2S_5 initial catholyte could liberate ~16 mg of Na during the electrochemical oxidation (viz. charging) of $Na_2S_5 \rightarrow Na_2S_8$. Hence, with an applied charging current of 7.5 mA, it takes 150 minutes to convert the catholyte's phase from Na_2S_5 to Na_2S_8.

Re-configured cells to alter catholyte's layer thickness in-between BASE and outer casing

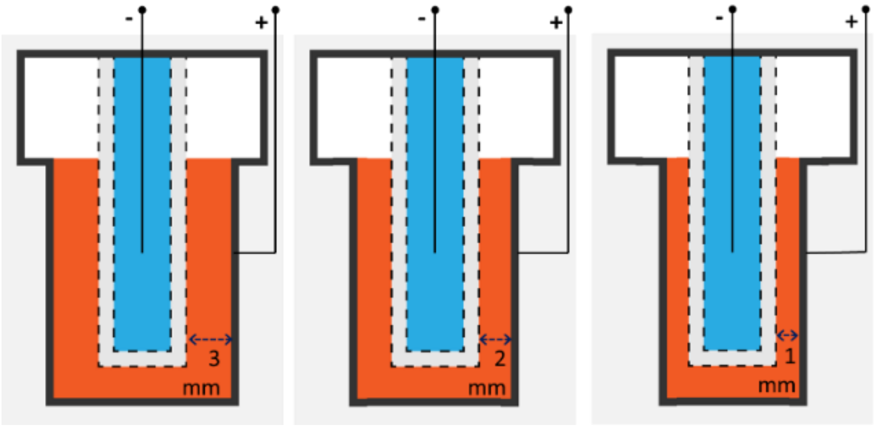

Figure S8. Cells with different catholyte layer thickness at BASE – cathodic current collector interface.

Concentrated catholytes and cells performance for session 2.7

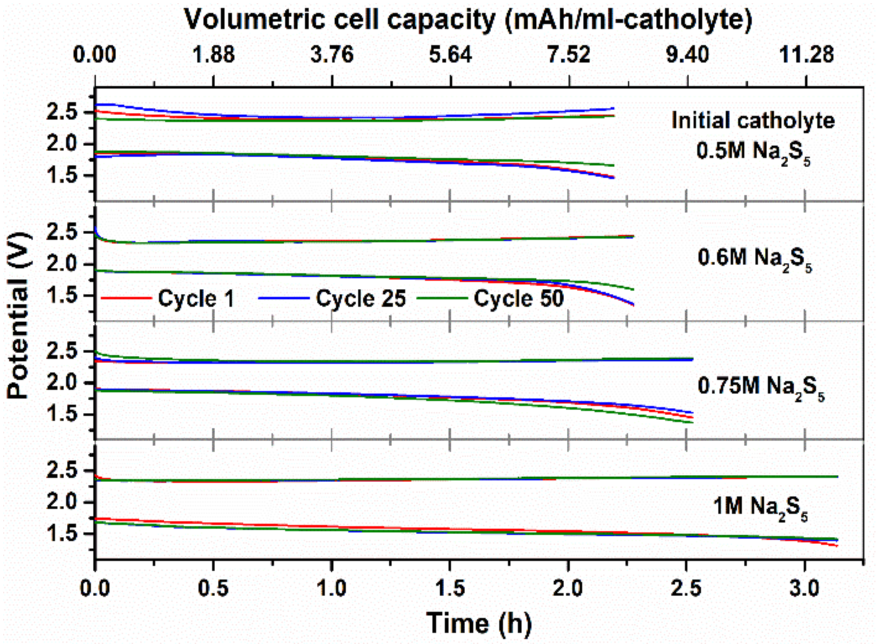

Figure S9. Time versus potential profile for the cells with different catholytes, but with the same layer thickness (1 mm).

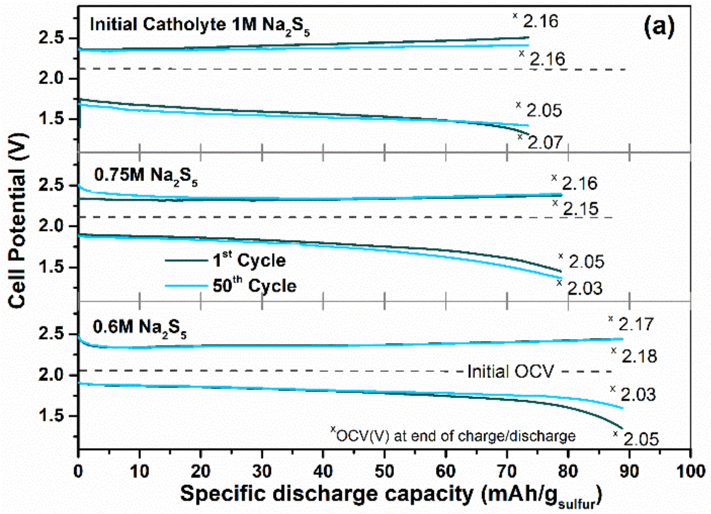

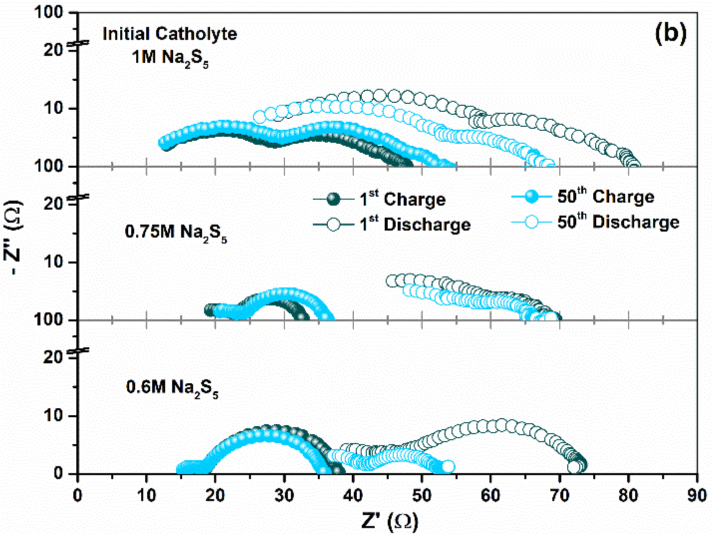

Figure S10. a) Charge-discharge and **b)** Nyquist plots of the cells with different initial catholyte concentrations (Na_2S_5) at 125 °C and 1 mm catholyte layer thickness.

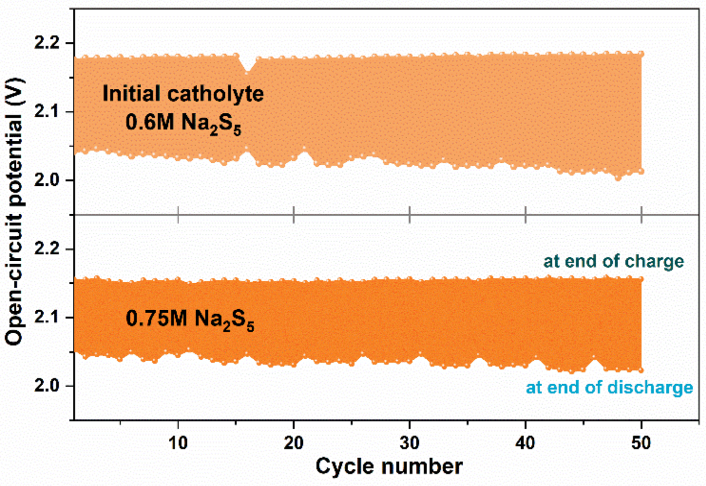

Figure S11. OCV at the end of charge and discharge for cells (1 mm thick layer) operated at 125 °C with different catholyte concentrations.

Cell performance efficiency calculation

The cell efficiencies summarized in Table 4 and Figure 10 are calculated as follows,[16]

$$\text{Coulombic efficiency } (\eta_C\,\%) = \frac{Q_{\text{discharge}}}{Q_{\text{charge}}} \times 100 \qquad \text{(S4)}$$

i.e., η_C is the ratio of the total charge extracted ($Q_{\text{discharge}}$) from the battery to the total charge put into (Q_{charge}) the battery over a full charge cycle.

$$\text{Voltaic efficiency } (\eta_V\,\%) = \frac{V_{\text{discharge}}}{V_{\text{charge}}} \times 100 \qquad \text{(S5)}$$

i.e., η_V is the ratio of the average discharging voltage ($V_{\text{discharge}}$) to the average charging voltage ($V_{\text{discharge}}$) of the cycle.

$$\text{Energy efficiency efficiency } (\eta_{\text{bat}}\,\%) = \eta_C \times \eta_V \qquad \text{(S6)}$$

Stability of the catholyte after 50 deep charge-discharge cycles

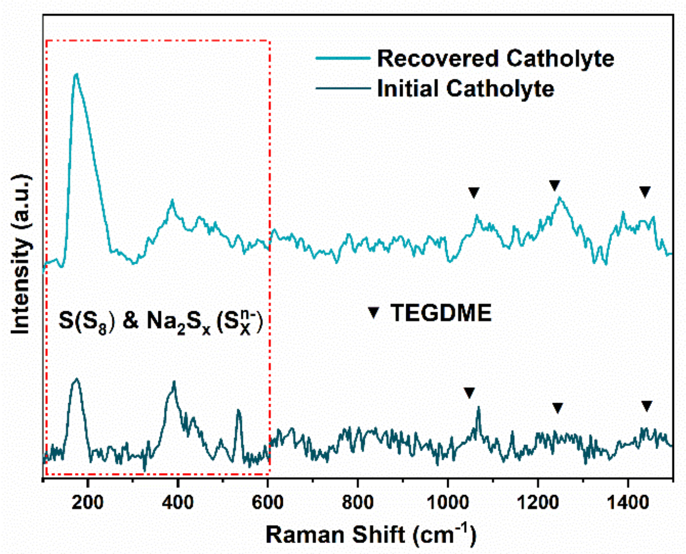

Figure S12. Raman spectrum of initial and recovered (after 50 cycles) catholyte (0.5M Na_2S_5) from the 1 mm thick catholyte layer cell operated at 125 °C.

Sampling for Raman spectroscopy

The sodium polysulfides (catholytes in Figure S13) are dark in colour and viscous. Hence, spectroscopic studies are difficult due to the intrinsic limitations in the opacity that saturate the detector.[25] To this end, samples were prepared by diluting a small fraction of the polysulfide in a suitable transparent solvent (e.g. 1 ml 0.5M Na_2S_5 in TEGDME (9 ml)). Diluting the catholyte in TEGDME changes the chemical composition due to further dissolution of the solute in solvent, and the resultant spectrum will not imitate precisely the one of the catholyte. To overcome this issue, the sampling process was modified by thinning the samples' thickness to the extent that it is sufficiently transparent for analysis. A few drops of catholyte were sandwiched between two quartz slides and subjected to the Raman analysis to obtain the exact chemical composition of the catholyte (fresh and recovered).

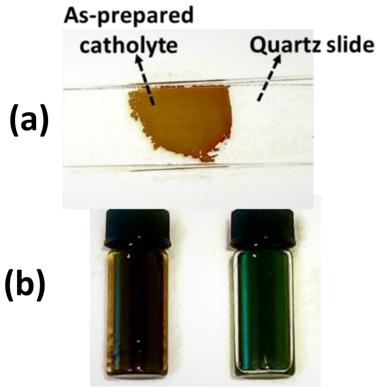

Figure S13. a) Raman sampling in this study, catholyte sandwiched between two quartz slides. **b)** Initial catholyte 0.5M Na_2S_5 as-prepared (left), diluted as 1 ml in 9 ml of TEGDME (right).